An Update to Probable Maximum Precipitation Accounting for More than Moisture Availability Alone: A Case Study of Nepal

ASPHOTA WASTI,[a,b] KATHERINE SCHLEF,[c] BILL KAPPEL,[d] SAIFUL HAQUE RAHAT,[e] GAURAV ATREYA,[a] GARIMA MANDAVYA,[a] AMY TOWNSEND-SMALL,[f] AND PATRICK RAY[a]

[a] *Department of Chemical and Environmental Engineering, College of Engineering and Applied Science, University of Cincinnati, Cincinnati, Ohio*
[b] *HDR Engineering Company, Sacramento, California*
[c] *Department of Civil and Environmental Engineering, College of Engineering, Western New England University, Springfield, Massachusetts*
[d] *Chief Meteorologist, Applied Weather Associates, Monument, Colorado*
[e] *WSP in the US, Environmental Consulting Company, New York, New York*
[f] *School of Environment and Sustainability Studies, College of Arts and Sciences, University of Cincinnati, Cincinnati, Ohio*

(Manuscript received 8 November 2024, in final form 22 April 2025, accepted 5 May 2025)

ABSTRACT: Probable maximum precipitation (PMP) in most cases determines probable maximum flood, which is the design flood for critical infrastructure such as dams and power plants, where failures are considered unacceptable. The moisture maximization approach, a common technique for estimating PMP, assumes that the upper limit of extreme precipitation can be determined by maximizing atmospheric moisture availability, while keeping the storm dynamics and thermodynamics unchanged. In this paper, a generalization to the moisture maximization approach is proposed that 1) identifies other relevant atmospheric variables and 2) incorporates them in the PMP calculation, using a two-step multifactor maximization approach. In the first step, the influence on historical extreme precipitation of each of atmospheric stability, atmospheric humidity, large-scale wind convergence, moisture availability, mean air temperature, temperature gradient, wind direction, and wind magnitude is evaluated to screen the dominant variables. In the second step, the maximization ratio for each variable is calculated separately, and the combined maximization ratio is obtained as a weighted average of the individual maximization ratios. This approach is illustrated with a case study of Nepal. The multifactor maximization approach results in PMP estimates substantially different (up to 4×) from the conventional moisture maximization approach in regions where the PMP is particularly sensitive to factors other than atmospheric moisture availability. As global warming directly affects atmospheric variables accounted for in the multifactor maximization approach described here, this study has implications at the intersection of infrastructure development, climate risk assessment, and hydrology.

SIGNIFICANCE STATEMENT: Designing resilient infrastructure like dams relies on accurate probable maximum precipitation (PMP) estimates. Traditional PMP methods focus on atmospheric moisture, potentially missing critical atmospheric influences. This study introduces a multifactor approach that includes variables such as atmospheric stability and wind patterns, resulting in PMP estimates up to 4 times higher in regions like Nepal. By incorporating broader climate factors, this method enhances climate-resilient infrastructure planning.

KEYWORDS: Extreme events; Precipitation; CAPE; Climate

1. Introduction

Between 1970 and 2019, flood- and storm-related hazards accounted for 50% of all disasters and 45% of all reported deaths from disasters. The number of people exposed to floods globally has risen from 28.1 million in 1970 to 35.1 million in 2020, an increase of 24.9%; the number of recorded flood-related disasters 2000–19 increased by 134% relative to 1980–99 (UNDRR 2025). Floods cause more damage to property and result in more loss of human life than any other type of natural disaster (IFRC 2015). Floods are known to deteriorate water quality (Behzadi et al. 2022; Michalak 2016; Rahat et al. 2023) and threaten human health (Ding et al. 2019; Liang and Messenger 2018).

With climate change, intensification of extreme precipitation has already been observed (Fischer and Knutti 2016; Rahat et al. 2024; Li et al. 2025) and is projected to continue (Trenberth 2011; Nazarian et al. 2022; Coelho et al. 2022). In many regions of the world, this intensification of extreme precipitation poses risks to water infrastructure (e.g., dams, levees) (Chen and Hossain 2018; Wasti et al. 2022; Jeuken et al. 2023). Existing approaches to climate change risk assessment in the water sector are underdeveloped on the topic of flood risk (Ray et al. 2019; Rodríguez et al. 2021). Initial efforts to improve flood risk assessments have, for example, combined hydrologic models with weather generators. These generators are effective in reproducing climate drivers responsible for extreme precipitation, which are tied to large-scale thermodynamic and dynamical

Denotes content that is immediately available upon publication as open access.

Supplemental information related to this paper is available at the Journals Online website: https://doi.org/10.1175/JHM-D-24-0152.s1.

Corresponding author: Patrick Ray, raypk@ucmail.uc.edu

DOI: 10.1175/JHM-D-24-0152.1

shifts that we can reasonably rely on Rahat et al. (2022), Steinschneider et al. (2019), and Kucharski et al. (2024). A primary cause of difficulty in our ability to confidently assess flood risks under climate change uncertainty is the deficit in our understanding of the behavior of extreme precipitation historically, even before accounting for climate nonstationarity. This paper aims to improve our fundamental understanding of extreme precipitation as a first step to understanding historical flood risk, which is a precursor to questions regarding the impacts of climate change on potential future flood behavior.

Dams are designed to resist or absorb the inflow design flood (IDF). The IDF is a flood magnitude typically estimated using either 1) the flood frequency analysis (FFA) or 2) the probable maximum flood (PMF) method. In rare cases, a rock–ice avalanche or glacial lake outburst might generate a flood magnitude large enough to dictate the inflow design flood (Fluixa-Sanmartin et al. 2018; Stoffel and Huggel 2012). In the following few paragraphs, we introduce the FFA and PMF approaches and discuss their application to water resource system infrastructure design under climate nonstationarity, especially dam design, worldwide.

The FFA method fits historical flow data to probability distributions and presents results in terms of "return periods" (e.g., 1-in-10 000-yr flood). FFA originated in 1914 with the use of plotting position to obtain site-specific estimates of flood (Fuller 1914). Several techniques to fit flood data to probability distributions were introduced in the following decades (Beard 1962; Foster 1924; Gumbel and Chow 1952). In 1966, the Subcommittee on Hydrology of the U.S. Interagency Committee on Water Resources released Bulletin 13 to "present a set of techniques for frequency analysis that is based on the best of known hydrological and statistical procedures" and to maintain uniformity across U.S. government agencies (ICWR 1966). Subsequent bulletins have been released over time; the latest version is Bulletin 17C (England et al. 2019). Readers interested to learn more about the evolution of FFA applied to water resource system infrastructure design are referred to Thomas (1985) and Dawdy et al. (2012).

The PMF approach, on the other hand, uses physics-based laws of hydrometeorology to estimate the inflow design flood. Before the 1950s, the deterministic approach was envisioned as a zero-risk design approach with the ability to determine the maximum possible precipitation (MPP) with absolute certainty (Salas et al. 2020). With the collection of more data over time, and improvement in the understanding of atmospheric science and dynamics of the climate system, uncertainty in the MPP was acknowledged, and the term probable maximum precipitation (PMP) was coined. PMP is defined as "the greatest depth of precipitation for a given duration meteorologically possible for a design watershed or a given storm area at a particular location at a particular time of year, with no allowance made for long-term climatic trends" (WMO 2009). In the United States, the National Oceanic and Atmospheric Administration's (NOAA) Hydrometeorological Report (HMR) series provides guidelines for PMP estimation specific to each region of the country (NWS 2015). With newer events, the storm database and the PMP estimates associated with it have been updated over time (e.g., Kappel et al. 2022, 2023). NOAA is researching methods to modernize PMP estimates in the United States with findings anticipated to be released by the end of this decade (NASEM 2024). There are both hydrometeorological (US Weather Bureau 1960; Hansen et al. 1982) and statistical (Hershfield 1961, 1965) methods to PMP estimation. The focus of this paper is on hydrometeorological methods, for reasons primarily of interpretability and relevance to climate change risk assessment applications (further discussion). Readers interested to learn about the history and development of PMP are referred to Salas et al. (2020) and Mukhopadhyay and Kappel (2016).

In standard engineering texts, FFA is discussed in great depth, whereas the discussion of PMF is either completely left out (e.g., Loucks and van Beek 2017) or discussed only briefly (e.g., Maidment 1993; Mays 2010). There is a disconnection between the large role of PMF in the design of essential water infrastructure worldwide and its general neglect in the typical university curriculum.

The guideline "Selecting and Accommodating Inflow Design Floods for Dams" (FEMA P-94) recommends the FFA approach in the United States for low–medium hazard potential and PMF for structures with high hazard potential (FEMA 2013). The standards are similar in other countries, where PMF is recommended for the most severe category of hazard, and other methods (including FFA) are recommended for the lower categories of hazard (ICOLD 2018). The PMF approach does not explicitly evaluate the degree of confidence in the estimate (Zielinski 2009). Consequently, some locations in the United States (e.g., California, Washington D.C., Montana) have adopted a risk-informed analysis (FEMA 2013), arguing that the "greater effort required for risk-based methods is frequently justified to allow more integrated consideration of water resource management objectives and tradeoffs." The risk-based design paradigm is appropriate for the avoidance of likelihood-weighted vulnerabilities of one type (or to one population), which might be traded off against vulnerabilities of other types (or to other populations) (e.g., Loucks et al. 1981). The FFA approach fits this paradigm well. However, when the goal is to avoid unacceptable catastrophe, a scenario-based (nonprobabilistic) approach to project vulnerabilities is typically preferred (Marchau et al. 2019). The PMF approach supports design objectives of this type.

Therefore, owing to its approach to vulnerability management, as well as its interpretability, low cost, and direct link to physical climate science, PMF remains the global standard for the selection of IDF for dams and other water resource system infrastructure with high hazard potential, the failure of which may cause severe loss of life and property. There is the further consideration (discussed briefly in the conclusion) that the application of probabilistic flood estimation techniques under climate nonstationary is highly complex, and by linking more directly to physical climate change phenomena, hydrometeorological PMP estimation techniques may be the more rational approach to PMF estimation under climate change uncertainty. In this paper, we address only hydrometeorological PMP and not probabilistic approaches to flood estimation.

The hydrometeorological estimation of PMP starts with identification of the local historical extreme precipitation events followed by correlations to the associated atmospheric

variables. Exploration is then made to determine if relaxing the limiting conditions of the atmospheric variables could result in a higher amount of precipitation (Salas et al. 2020). Of the several methods to estimate PMP under historical and climate change–altered conditions, there has recently been a proliferation of studies applying the moisture maximization approach (Beauchamp et al. 2013; Chen et al. 2017; Lee et al. 2016; Micovic et al. 2015; Rouhani and Leconte 2018; Rousseau et al. 2014). This approach assumes that extreme precipitation is limited by a single atmospheric variable: precipitable water (PW), or atmospheric moisture, and estimates the PMP by maximizing PW as shown in Eq. (1):

$$\mathrm{PMP}_{\mathrm{moisture\_maximization}} = P_{\max} \times \frac{\mathrm{PW}_{\max}}{\mathrm{PW}_{P_{\max}}} = P_{\max} \times r_{\mathrm{PW}}, \tag{1}$$

where $P_{\max}$ is the maximum observed precipitation depth (mm) for a location and time of the year, $\mathrm{PW}_{P_{\max}}$ is the PW during the maximum observed precipitation (mm), $\mathrm{PW}_{\max}$ is the maximum PW (mm) observed at the same time of year and the same location, and r_{PW} is the unitless moisture maximization ratio (WMO 2009).

Despite the focus on PW, extreme precipitation could be affected nonuniformly by several factors simultaneously. Yang and Smith (2018) recreated an extreme precipitation event in Arizona with an atmospheric model and showed that the response of extreme precipitation to an increase in atmospheric moisture is nonlinear, suggesting the influence of other factors beyond atmospheric moisture alone. In the Netherlands, large-scale velocity and stability parameters were found to have a positive influence on extreme precipitation (Loriaux et al. 2016). In a study of the conterminous United States, several relationships that highlight the significance of dewpoint temperature and convective available potential energy (CAPE) on extreme precipitation were found (e.g., Lepore et al. 2015).

Atmospheric simulation numerical modeling studies (e.g., Rastogi et al. 2017; Yang and Smith 2018) represent a new third category of approach to PMP estimation, in addition to the hydrometeorological (US Weather Bureau 1960; Hansen et al. 1982) and statistical (Hershfield 1961, 1965) categories introduced above. Numerical modeling studies, e.g., Hiraga et al. (2021) and Tarouilly et al. (2024), apply atmospheric simulation techniques that better capture the dynamics of extreme precipitation events. Hiraga et al. (2024a) extended these models to incorporate large basins and reservoirs, improving design precipitation estimates for infrastructure projects reliant on snowpacks and large storage volumes. Rastogi et al. (2017) and Hiraga et al. (2024b) provided evidence of nonlinearity between precipitation and atmospheric moisture, and others have incorporated aspects of PMP stochasticity (e.g., Ben Alaya et al. 2018; Papalexiou 2018). Advanced numerical modeling experiments such as these demonstrate the complexity of extreme precipitation dynamics and the importance of considering multiple factors simultaneously in modeling such events; however, their techniques are not commonly adopted by water resource engineering design firms or institutions responsible for civil infrastructure planning.

The interest of this paper is to scrutinize the comprehensiveness of the widely adopted ("operational" or conventional) moisture maximization approach for PMP estimation (as opposed to the statistical- or numerical-modeling-based techniques) and propose an extension to the technique that includes additional atmospheric variables using a multifactor maximization approach. Chen and Hossain (2018) extracted spatial and seasonal patterns of the influence of a diversity of atmospheric processes on extreme precipitation. Their technique not only was developed with a case study of the continental United States but has also been applied to understand the controlling factors for extreme precipitation in central China (Lang et al. 2022). Building on the work of Chen and Hossain (2018), we introduce a PMP estimation algorithm that 1) identifies the dominant atmospheric drivers of extreme precipitation and 2) uses the relevant variables (weighted by their influence) to develop a revised, multifactor estimate of PMP.

The moisture maximization approach is univariate and has a simple mathematical form. An accurate representation of a "storm" would require several variables and highly nonlinear complex mathematical formulation. In the multifactor maximization approach, a trade-off is made between simplicity and accuracy by using a multivariate approach with a linear combination of the variables. In the proposed approach, on the one hand, the dominant variables (and their weights) capture the complex nature of storms, and on the other hand, the linear combination retains much of the simplicity of the conventional moisture maximization method. Because the moisture maximization approach relies solely on a single variable, its accuracy is constrained by the extent to which the variability in moisture content accounts for the variance in precipitation. By including other relevant atmospheric variables, the approach presented here improves the explanatory power of the equation.

The paper is organized as follows: Section 2 presents the methodology; section 3 introduces the case study, the dataset used, and the atmospheric variables explored; section 4 offers results, discussion, and limitations; and section 5 concludes.

2. Methodology

The multifactor maximization approach proposed in this paper is an expansion of the traditional moisture maximization approach (WMO 2009). The approach consists of two processes: 1) the screening process and 2) the maximization process. Each process is described here in detail.

a. The screening process

In the screening process, we identify the dominant atmospheric variables that drive the extreme precipitation for a given location and time of the year. We employ the approach proposed by Chen and Hossain (2018) to identify the drivers of extreme precipitation. First, the extreme precipitation events are identified, and the associated atmospheric variables (PW, relative humidity, air temperature, CAPE, and components of wind velocity) are extracted from a time series of meteorological variables (e.g., a reanalysis dataset). In the screening process, two

parameters are defined: 1) the number of events to be studied (N) and 2) the threshold of the extreme precipitation event (θ). The sensitivity of the result to the choice of these parameters is unique to each study. For this case study, the sensitivity analysis is presented in section 4a(2).

Once the data are collected, an empirical cumulative distribution function (CDF) is fitted to the values in the entire period of record for each variable. For an atmospheric variable i and an extreme precipitation event j, the metric M indicating the concurrence of the extreme precipitation i and the atmospheric variable j is defined as shown in Eq. (2):

$$M_i^j(\theta) = P(X_i^j > X_i^\theta), \tag{2}$$

where X_i^j is the value of the atmospheric variable i during the jth extreme precipitation event; N is the total number of extreme events investigated ($N = 50$ in this study); and X_i^θ is the value of the atmospheric variable i corresponding to the quantile estimate associated with θ ($\theta = 0.90$ is adopted in this study), which is the percentile cutoff for the extreme condition. The weight w_i for each atmospheric variable i is then expressed in Eq. (3) as

$$w_i = \sum_{j=1}^{N} \frac{M_i^j(\theta)}{N}. \tag{3}$$

This process is repeated for each grid, and thus, a weight is calculated for every grid of the reanalysis dataset for each atmospheric variable. At the end of this process, the dominant atmospheric variables i are selected based on their corresponding weights w_i.

b. The maximization process

In the maximization process, we estimate the maximization ratio for each atmospheric variable and then calculate the combined maximization ratio. For an atmospheric variable i and an extreme precipitation event j, the maximization ratio r is calculated using Eq. (4) as

$$r_{\mathrm{i}} = \frac{\mathrm{Max}\,(X_i^j)}{X_i^{j_{\max}}}, \tag{4}$$

where $\mathrm{Max}(X_i^j)$ is the maximum value of the atmospheric variable i for the given location and the given time, derived from the historical record. The $X_i^{j_{\max}}$ is the value of the atmospheric variable i during the maximum precipitation event $j_{\max}$.

The individual maximization ratios are then combined to obtain a combined maximization ratio r_{combined} as the weighted average of the maximization ratios r_i's using Eq. (5):

$$r_{\mathrm{combined}} = \frac{\sum_1^n w_i r_i}{\sum_1^n w_i}, \tag{5}$$

where n is the number of atmospheric variables selected for the maximization ($n = 4$ in this study). Finally, the PMP estimation with the multifactor maximization is proposed in Eq. (6) as

$$\mathrm{PMP}_{\mathrm{multifactor\_maximization}} = P_{\max} \times r_{\mathrm{combined}}. \tag{6}$$

The proposed formula is a linear expansion of the conventional moisture maximization approach to include other atmospheric variables beyond PW, weighted by their relative importance for the location of interest. The proposed multifactor maximization approach reduces to the moisture maximization approach when precipitable water is the only driving atmospheric variable and its weight is 1. Additionally, it assumes independence among the contributing factors, though this assumption may not always hold. For instance, in this study, two of the selected drivers were found to be moderately correlated—a point discussed in detail in a later section.

The choice of a linear expansion is motivated by simplicity, interpretability, and reproducibility. While it is possible to consider nonlinear expansions, such as polynomial or exponential relationships, these models are more complex and less interpretable, especially if the relationship between the variables is not well understood.

3. Case study and data used

a. Case study: Nepal

In Nepal, on average, floods and landslides are the causes of over 175 deaths and economic losses exceeding 140 million U.S. dollars each year (ADB 2019). In terms of relative physical exposure to river (fluvial) flooding, Nepal ranks tenth in the world, with potential damage to physical assets amounting to 1.4% of its GDP (WRI 2015).

Our discussion of the dynamics of PMP has focused so far on the United States and China, where extensive literature is available. Similar explorations of PMP dynamics are not available throughout much of the world, resulting in a substantial gap in understanding. In part to address this research gap, we selected Nepal as our case study. As a South Asian country situated along the southern belt of the central Himalayas, Nepal is home to over 6000 rivers and rivulets (Agrawala et al. 2003), making it a crucial region for studying extreme precipitation events.

Nepal receives an average annual precipitation of about 1000 mm, of which 50%–90% is supplied by the summer monsoon precipitation within 3–4 months (Bohlinger and Sorteberg 2018). Winter storms moving through the northwest part of the country provide a minor contribution to the annual precipitation. The summer monsoon precipitation is highly variable and is modulated by long-term climate drivers, including the Pacific quasi-decadal oscillation (Wang and Gillies 2013) and El Niño–Southern Oscillation (Kumar et al. 1999; Shrestha et al. 2000; Sigdel and Ikeda 2012). However, the influence of these large oscillations on precipitation diminishes at higher percentiles, and historically, extreme precipitation above the 90th percentile is found to be independent of the effects of long-term climate drivers (Bohlinger and Sorteberg 2018).

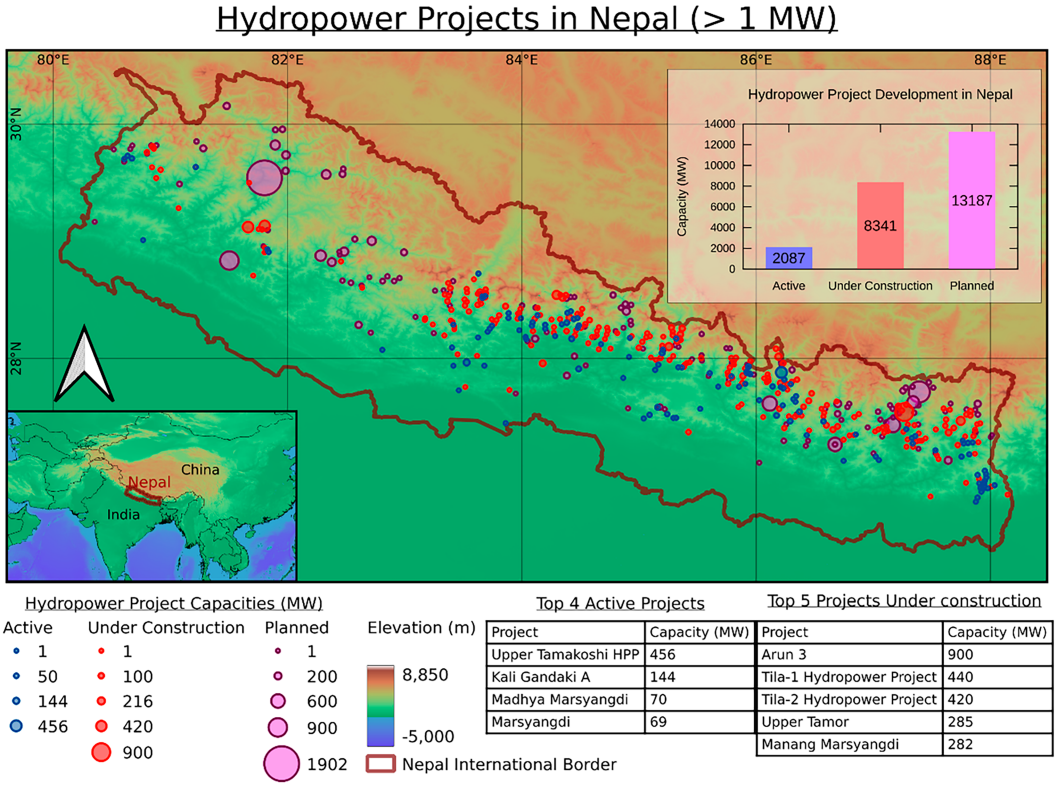

Project	Capacity (MW)
Upper Tamakoshi HPP	456
Kali Gandaki A	144
Madhya Marsyangdi	70
Marsyangdi	69

Project	Capacity (MW)
Arun 3	900
Tila-1 Hydropower Project	440
Tila-2 Hydropower Project	420
Upper Tamor	285
Manang Marsyangdi	282

FIG. 1. Elevation information of Nepal and the location and size of hydropower plants in Nepal. Data source: Department of Electricity Development (2022).

Hydroelectricity is the major source of energy in Nepal. With an elevation range from 60 to 8848 m MSL, more than 90% of Nepal's electricity is supplied by hydroelectric power. The current installed capacity of 2 GW is expected to increase to 10 GW after the completion of the underconstruction hydropower plants, and over 13 GW more are being planned for the future (see Fig. 1). Previous climate change risk assessments of hydropower projects in Nepal have focused on questions of change to water balance instead of questions of change to precipitation extremes (Hurford et al. 2020; Ray et al. 2018; Wasti et al. 2022). As the country is expanding its water infrastructure at such a rapid pace, the need for improved PMP estimates is current.

b. *Dataset: ERA5*

ERA5 is the fifth generation European Centre for Medium-Range Weather Forecasts atmospheric reanalysis that provides long time series of atmospheric fields at high spatial and temporal resolution (Hersbach et al. 2020). It is an update on the ERA-Interim product (Dee et al. 2011) and provides better precipitation estimates in China and Tibet (Tang et al. 2020). The ERA products have been used for evaluating extreme precipitation and related atmospheric variables in several PMP studies (Ben Alaya et al. 2019; Chen and Hossain 2018). PW estimates from the reanalysis dataset show good agreement with radiosonde observations in Tibet and China (Zhang et al. 2019). ERA products have also been used to estimate the change in moisture flux and moisture convergence for extreme precipitation in the South Asian monsoon system (Suman and Maity 2020) and to map the moisture sources and synoptic conditions for extreme precipitation in Nepal (Bohlinger et al. 2017).

Despite its coarse resolution, ERA5 is a valuable dataset for explorations of relative changes to extreme precipitation, particularly in data-scarce regions such as Nepal, where high-resolution observational records are limited. Previous studies have demonstrated that ERA5 effectively captures large-scale meteorological patterns associated with extreme precipitation, indicating its relevance for analyses of PMP-related atmospheric conditions (Liu et al. 2024; Lavers et al. 2022). Previous studies, such as Khadka et al. (2022), who evaluated ERA5-Land data in the Everest region, and Luo et al. (2024), who examined changing extreme precipitation patterns in Nepal using ERA5, have demonstrated its applicability for understanding extreme precipitation in the region. In this analysis, hourly ERA5 data for 1979–2019 were aggregated to daily values.

PMP is specific to a given location and time of the year and is often estimated for a 3-day or a 72-h duration (Chen and Hossain 2018; Rastogi et al. 2017; Rousseau et al. 2014). The duration of PMP estimates is dependent on the critical duration of the PMF for a given location. This can range from less than an hour for small or steep basins to several days for large, slow-responding basins. In Nepal, the maximum 3-day

precipitation occurs in June–August during the summer monsoon precipitation (see in the online supplemental material). Thus, we base our PMP estimate in this study on the 3-day precipitation June–August 1979–2019.

c. *Atmospheric variables*

The influences of the following atmospheric variables on extreme precipitation are explored in this study.

1) CAPE (J KG^{-1})

CAPE is the measure of the amount of energy available for convection, which, in meteorological terms, represents the upward movement of warm air. It is an indication of the instability of the atmosphere and can be used to assess the potential for the development of heavy rainfall, thunderstorms, and other severe weather. CAPE has been established as an important driver of extreme precipitation (Chen and Hossain 2018; Lang et al. 2022; Lepore et al. 2015). This study uses the CAPE estimates directly from the ERA5 reanalysis dataset.

2) PW (MM)

PW, also sometimes known as precipitable water vapor, is the amount of liquid water that would be obtained if all the vapor in the atmosphere within the vertical column were compressed to the point of condensation (Dupont et al. 2008). PW is an indicator of moisture availability in the atmosphere and is the basis of the moisture maximization approach.

In this study, we use Eq. (7) to estimate PW, as proposed by Zhang et al. (2019):

$$\mathrm{PW} = \sum_{i}^{n-1} \frac{(q_i + q_{i+1}) \times (p_{i+1} - p_i)}{2\rho_w \times g}, \tag{7}$$

where q_i is the specific humidity (kg kg^{-1}) and p_i is the air pressure (Pa) at the layer i, ρ_w is the density of liquid water (ρ_w = 1000 kg m^{-3}), g is the acceleration due to gravity (g = 9.81 m s^{-2}), n is the total number of layers between pressure level P_1 and P_2, P_1 is the pressure at the sea surface level, and P_2 is the pressure at the upper level of the atmosphere. In this study, PW is calculated using specific humidity between P_1 = 1000 hPa and P_2 = 100 hPa at 50-hPa intervals.

3) RH (–)

Relative humidity (RH) is the amount of water vapor present in air, expressed as a percentage of the amount needed for saturation at the same temperature. In meteorology, the dewpoint temperature is often discussed together with relative humidity. Dewpoint temperature is the temperature at which the air becomes water saturated. Both relative humidity at different pressure levels and dewpoint temperature are important variables in the PMP estimation (Ishida et al. 2018; Lee and Kim 2018; Lepore et al. 2015; Stratz and Hossain 2014). In this study, we use the relative humidity directly from the ERA5 reanalysis dataset at 850-hPa pressure level as RH.

4) AIR TEMPERATURE (T_{AVG} AND T_{DIFF}) (K)

Air temperature could also play a key role in extreme precipitation. The role of air temperature in the evolution of an extreme precipitation event has been explored (Chen and Hossain 2018; Lepore et al. 2015). An increase in air temperature under climate change is projected to increase the PMP in the future (Ishida et al. 2018; Kunkel et al. 2013). In this study, we use the air temperature values from the ERA5 reanalysis dataset. We defined two variables, general air temperature (T_{avg}) and vertical temperature gradient (T_{diff}), to represent the air temperature. As introduced by Chen and Hossain (2018), T_{avg} is the average air temperature between 850 and 500 hPa and T_{diff} is the difference in air temperature between 850 and 500 hPa.

The selection of T_{avg} and T_{diff} is further supported by their relevance in capturing atmospheric instability and potential energy, similar to the role of pressure gradients in driving air and moisture movement. This approach aligns with previous research demonstrating the correlation between large-scale atmospheric circulation patterns and precipitation. For example, anomalies in geopotential height at 500 hPa (Najibi et al. 2021; Steinschneider et al. 2019), 700 hPa (Robertson and Ghil 1999), and sea level pressure (Corte-Real et al. 1998) have been linked to both the distribution and intensity of precipitation. In particular, high 500-hPa geopotential height anomalies near a focus region have been shown to coincide with extreme precipitation events. The use of temperature-based variables such as T_{avg} and T_{diff}, therefore, reflects both empirical precedent and physical reasoning in the context of extreme precipitation analysis.

5) COMPONENTS OF WIND VELOCITY (U_{WIND}, AND V_{WIND}) (M S^{-1})

The speed and the direction of the wind influence extreme precipitation. The flow of moisture-bearing wind against a mountain range or the funneling of wind in narrowing valleys and canyons may initiate or increase rainfall due to horizontal convergence and resultant vertical lift (WMO 2009). Wind velocity is used in the estimation of PMP either through a wind-moisture maximization factor (Boota et al. 2018) or with the use of a wind-rose diagram (Zhou et al. 2020). In this study, we use the wind velocity from the ERA5 reanalysis dataset. We use two variables, the eastward component of wind velocity (U_{wind}) and the northward component of wind velocity (V_{wind}) at 850 hPa, to represent wind.

Each of these variables influences atmospheric processes during an extreme precipitation event. Although the relationship between the variables and the precipitation is not linear, a monotonic relationship is observed (see supplemental material). The increasing monotonic relationship observed in the data gives credibility to the maximization approach adopted in (6).

4. Results and discussion

a. *The screening process*

Our analysis is based on the frequency analysis approach developed by Chen and Hossain (2018). While their analysis was based on subdaily observations, we aggregated the hourly

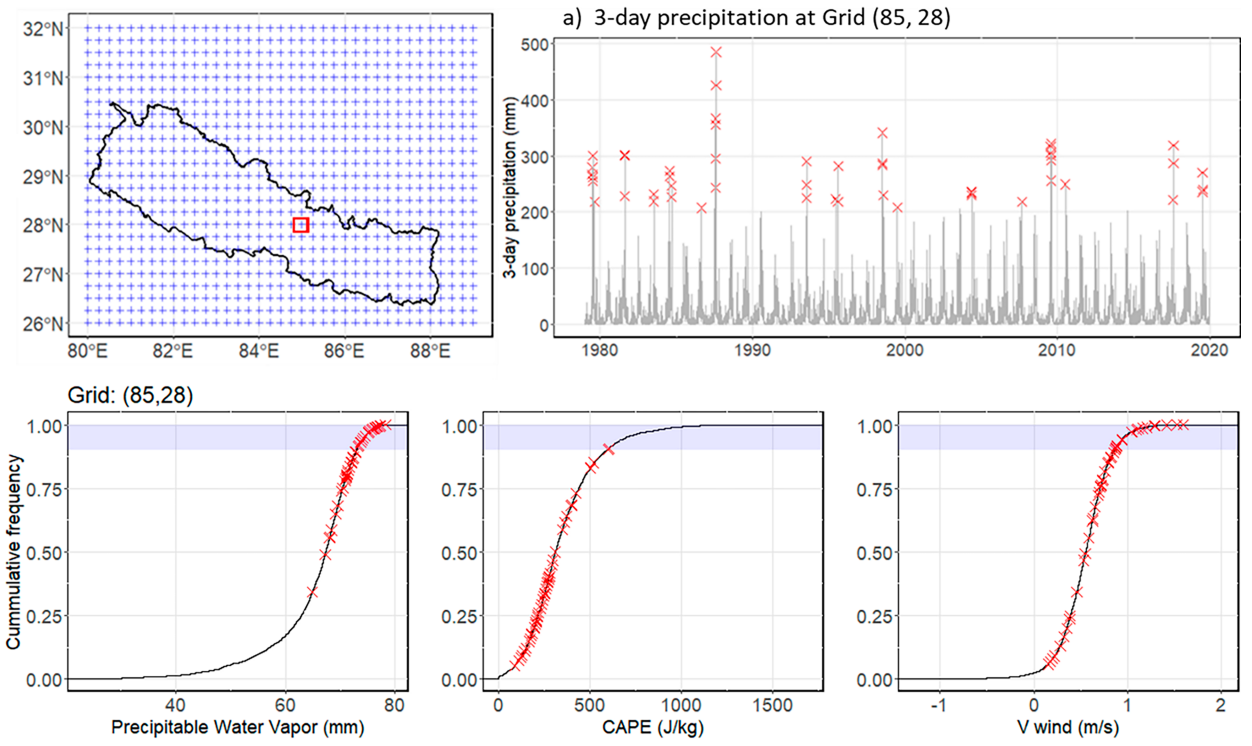

FIG. 2. Demonstration of the screening process. From a given grid, such as the one enclosed in a red box in the top left (26°N, 86°E), we obtain the top 50 3-day precipitation (marked by the red cross in the top right). The CDF of the atmospheric variables (PW, CAPE, and V_{wind} are shown here) is drawn that are unique for each grid ($n = 3731$). The red x marks on the CDF curves are the observed values of atmospheric variables corresponding to the top 50 3-day precipitation. We define the 90th percentile on the CDF curve (blue shaded region) as the threshold of the extreme condition. The proportion of red x marks lying within the threshold is recorded as weights ($w_{\text{PW}} = 0.48$, $w_{\text{CAPE}} = 0.06$, $w_{V_{wind}} = 0.40$).

estimates from the ERA5 reanalysis dataset into 3-day estimates to calculate 3-day PMP.

The screening process is illustrated in Fig. 2 for a sample grid (28°N, 85°E). The 3-day total cumulative precipitation for the sample grid is presented for the years 1979–2019 in Fig. 2a, and the top 50 values are marked with a red "x". For every grid, and each atmospheric variable, an empirical CDF curve is drawn for June–July observations between 1979 and 2019 ($n = 91$ days per year $\times$ 41 years $= 3731$ data points). The process is demonstrated for PW, CAPE, and V_{wind} in Figs. 2a–c, respectively. The values of these atmospheric variables co-occurring with the top 50 values of 3-day precipitation are marked on their corresponding CDF curve with a red x. The proportion of the red x marks lying within the 90th percentile of atmospheric variable magnitudes (highlighted by the blue rectangle) is recorded for each atmospheric variable. In this example, the proportions are 0.48 for PW, 0.06 for CAPE, and 0.40 for V_{wind}.

The resultant proportion for each atmospheric variable represents its dominance/influence on the extreme precipitation event. A higher proportion indicates that the atmospheric variable is high (in the upper 10th percentile) during the top 50 extreme precipitation events. These proportions are mutually independent, i.e., the proportion of one atmospheric variable does not affect the proportion of another. The process described in the paragraph above is applied to each grid.

Figure 3 shows the spatial distribution of the proportion of the event in which the "high" values of the atmospheric variables (CAPE, PW, V_{velo}, RH, T_{avg}, T_{diff}, U_{wind}, and V_{wind}) co-occurred with extreme precipitation in Nepal. The high values of atmospheric variables are defined as values that lie above the 90th percentile in the CDF curve made separately for each grid and each variable as illustrated in Fig. 2. The atmospheric variables explored in Fig. 3 demonstrate the spatial pattern that depends on the elevation, latitude, and access to moisture in Nepal. A higher proportion (darker shade) indicates that the variables are usually at high values during an extreme precipitation event. We observe that CAPE is related to the extreme precipitation on the north side of the Himalayan ridge. PW correlates to extreme precipitation everywhere except for the mountain peaks. The high values of V_{wind} are observed during extreme precipitation events in the valleys in the midhills of Nepal, indicating northward wind and the advection of moisture at low levels in the extreme precipitation in those areas. RH is highly correlated to PW (see supplemental material) and thus is deemed to be redundant. The variables V_{velo}, U_{wind}, and T_{diff} exhibit weak relationship with extreme precipitation. Thus, at the end of the screening process, of all the variables explored, only PW, CAPE, V_{wind}, and T_{avg} were selected and their corresponding weights w_{PW}, w_{CAPE}, $w_{V_{\text{wind}}}$, and $w_{T_{\text{avg}}}$ were used in the multifactor maximization. The variance inflation factor (VIF) for each selected term (PW, CAPE,

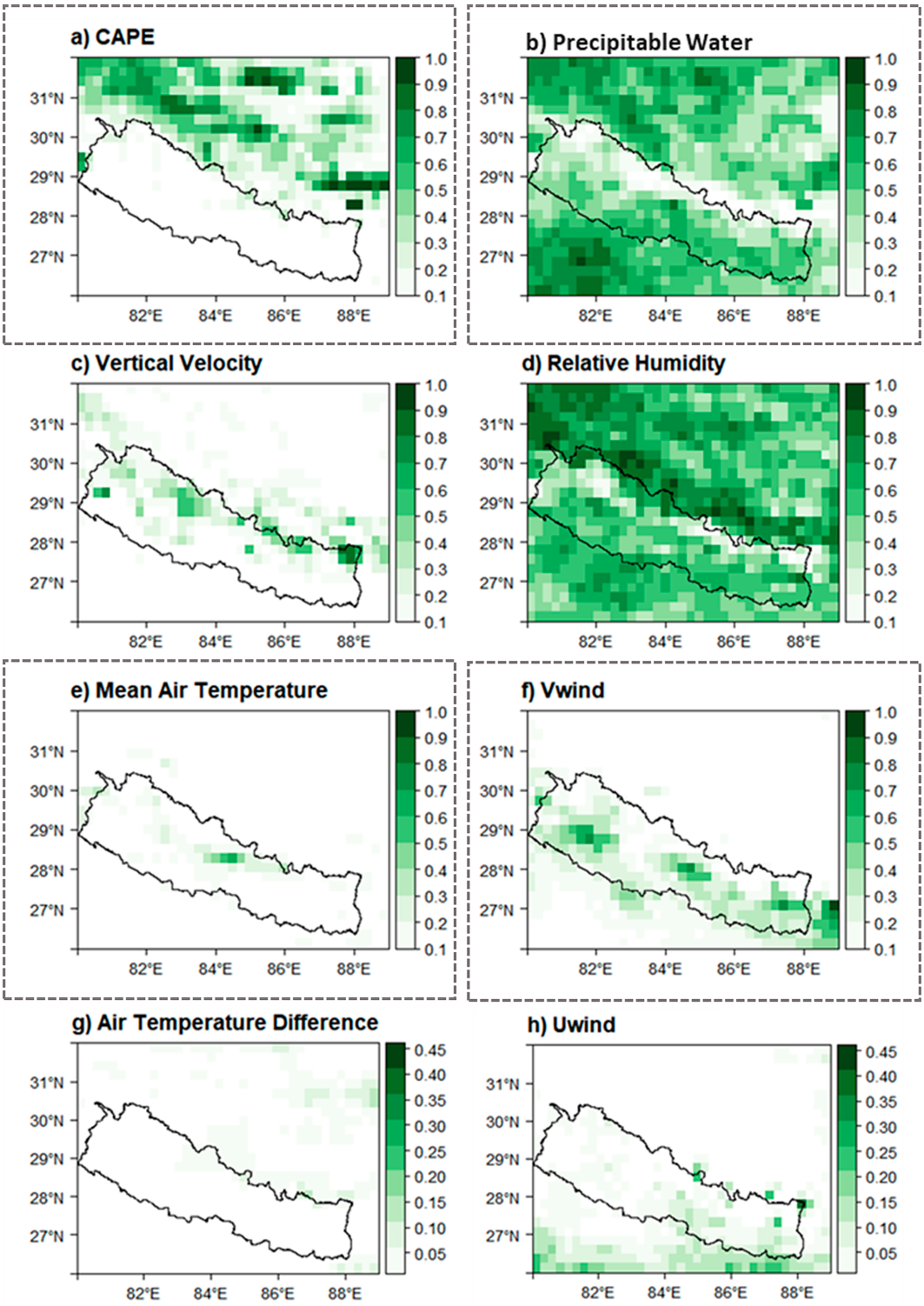

FIG. 3. (a)–(h) Relationship between the atmospheric variables (CAPE, PW, V_{velo}, RH, T_{avg}, T_{diff}, U_{wind}, and V_{wind}) and top 50 3-day extreme precipitation events. The saturation of color represents the proportions of high values of the atmospheric variable during historical storms. Note that the variables T_{avg} in (g) and U_{wind} in (h) are presented at a different scale (0–0.45). The variables selected with the screening process are emphasized with dotted lines.

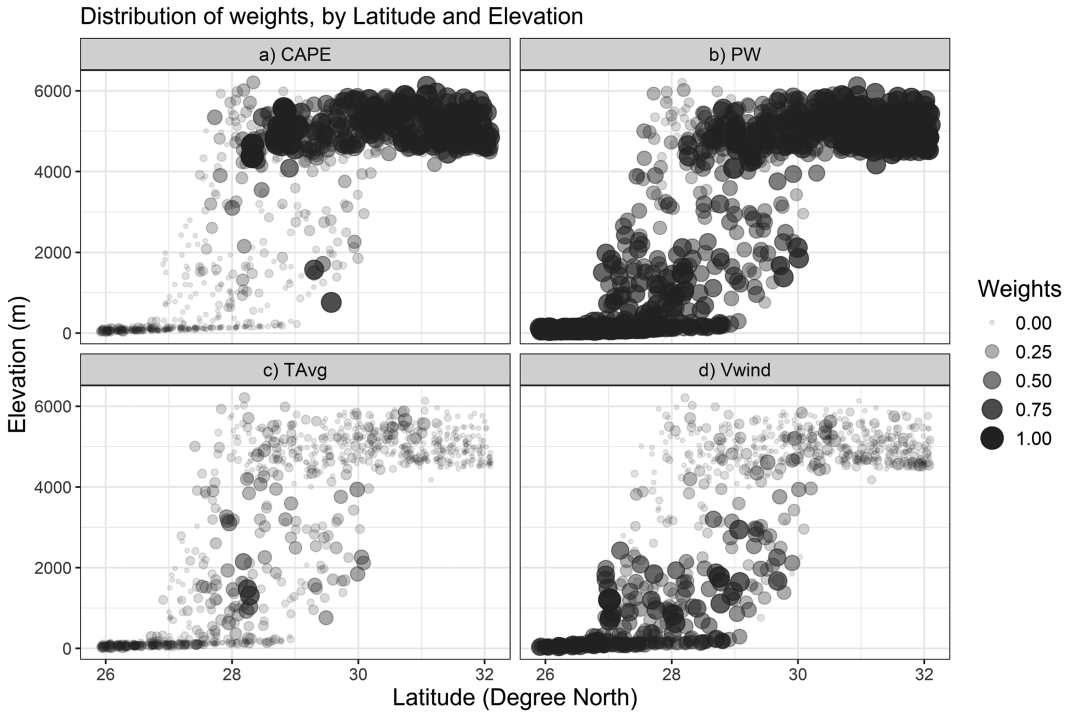

FIG. 4. Distribution of weights of dominant atmospheric variables by latitude and elevation.

V_{wind}, and T_{avg}) was ≥1, indicating that these terms to be highly uncorrelated. Although the influence of temperature $w_{T_{\text{avg}}}$ is minimal in the case of Nepal, it is included in this study for illustrative purposes and because it may be shown (in future studies) to be an important factor in other global regions. Its direct applicability to explorations of the impact of climate change on PMP also motivates its inclusion in the multifactor maximization equation adopted here.

The weights of the variable chosen are sensitive to the choice of 1) the number of historical events studied (N) and 2) the threshold of the extreme precipitation event (θ). A sensitivity analysis of the weights to the choice of these parameters is presented in section 4a(2). The spatial structure of the weights of the variable was also preserved when the screening process was repeated for a 1-day and a 2-day event (see supplemental material).

1) INTERPRETATION OF THE PATTERNS OF DRIVERS OF EXTREME PRECIPITATION

In this section, we analyze the spatial patterns of the weights of the dominant atmospheric variables. The weights of the variables are plotted against latitude and elevation to identify spatial patterns (Fig. 4).

(i) CAPE

CAPE indicates the (in)stability of the atmosphere. Higher CAPE represents a high potential for the development of convection (rise of warm air) and heavy rainfall, often accompanied by a thunderstorm. We observe that w_{CAPE} is high in elevation between 4000 and 6000 m. Topographically, this region is the area on the northern leeward side of the Himalayan Mountains (see Fig. 1). This is likely because there is a lack of sustained low-level moisture access in this region. Therefore, moisture at the mid- and upper levels of the atmosphere results in precipitation. However, to convert moisture in the mid- and upper levels of the atmosphere to precipitation on the ground, significant vertical motions through a large depth of the atmosphere, i.e., higher CAPE, is needed.

(ii) PW

PW is the most prominent driver of extreme precipitation. We observe that w_{PW} is generally high everywhere except in the elevation range of 2000–4000 m. Topographically, this elevation range represents the region between the foothills and the rising windward side of the Himalayas (see Fig. 1). Most likely, PW is not the dominant factor for extreme precipitation in this elevation range on the windward side of the Himalayas due to the higher influence of the orographic effect. In the leeward side of the Himalayas, both CAPE and PW drive extreme precipitation.

(iii) T_{avg}

The distribution of $w_{T_{\text{avg}}}$ is uniform and <0.25, with a few local exceptions. The low values of $w_{T_{\text{avg}}}$ suggest that the 3-day rolling average temperature by itself has the least influence on extreme precipitation. However, an increase (or decrease) in temperature has the potential to affect other atmospheric variables, which in turn may influence extreme precipitation.

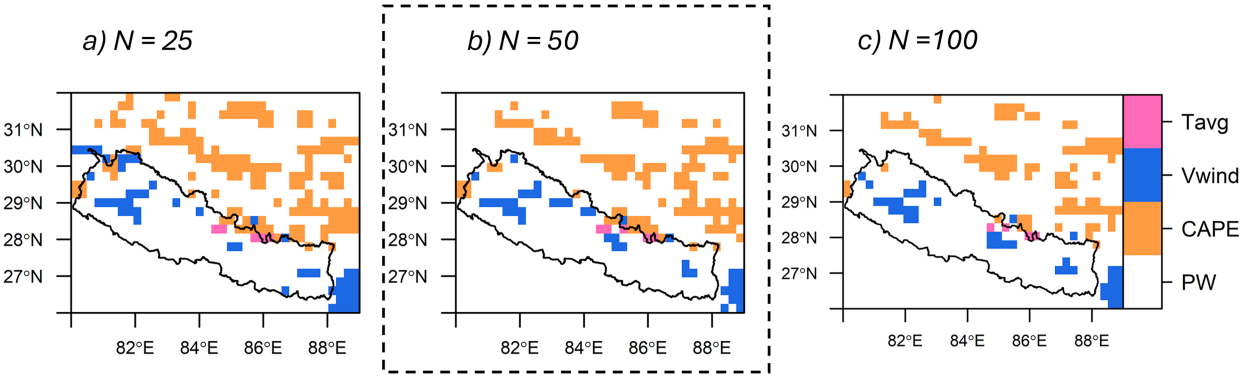

FIG. 5. Sensitivity of the most dominant atmospheric variable driving the 3-day extreme precipitation to the choice of number of events N. The variables PW, CAPE, V_{wind}, and T_{avg} are represented by the colors white, orange, blue, and pink, respectively.

(iv) V_{wind}

The values of $w_{V_{\text{wind}}}$ are observed to be high below 2000 m between 26° and 30°N. Topographically, this region (see Fig. 3) corresponds to the major valleys in the midhills of Nepal. During the Indian summer monsoon, moisture-laden winds flow northward toward the Himalayas. Wind flow in narrowing valleys may induce horizontal convergence and resultant vertical lift of moisture initiating or increasing precipitation (WMO 2009). These pockets of high $w_{V_{\text{wind}}}$ may indicate such phenomena.

2) SENSITIVITY ANALYSIS OF THE SCREENING PROCESS

The values and the spatial distribution of the weights of the dominant atmospheric variables are affected by the choice of the two parameters (θ and N).

We tested the sensitivity of our results to the choice of the number of historical events analyzed (N) by varying the number of events between 25 and 100. The most influential atmospheric variable with the maximum weight, max (w_i), is illustrated as N is set to (Fig. 5a) 25, (Fig. 5b) 50, and (Fig. 5c) 100, respectively, in Fig. 5. The sensitivity analysis indicates that the spatial distribution of the dominant atmospheric variable is preserved when the thresholds are varied. If N is set closer to 100, the criteria become overly generalized, and insights from the atmospheric variable are lost among other data noise. If we reduce the sample size nearer to 25, the criterion becomes overly restrictive and does not capture the natural variability of the atmospheric variables. For our study, the choice of 50 events ($N = 50$) was found to balance precision and inclusivity (emphasized with dotted lines in Fig. 5).

Similarly, we tested the sensitivity of the results to the choice of the threshold placed on the CDF curve (θ) by varying the threshold between the 85th and 95th percentile. The most influential atmospheric variable with the maximum weight, max (w_i), is illustrated as the threshold θ is set to 0.85 (Fig. 6a), 0.9 (Fig. 6b), and 0.95 (Fig. 6c), respectively, in Fig. 6. The sensitivity analysis indicates that the spatial distribution of the dominant atmospheric variable is preserved when the thresholds are varied. The choice of the 95th percentile is overly restrictive, and the 85th percentile is overly general. For our study, the choice of the 90th percentile ($\theta = 0.90$) was found to balance precision and inclusivity (emphasized with dotted lines in Fig. 6).

b. The maximization process

Once the screening process is complete, the maximizing process is performed. In the multifactor maximization approach,

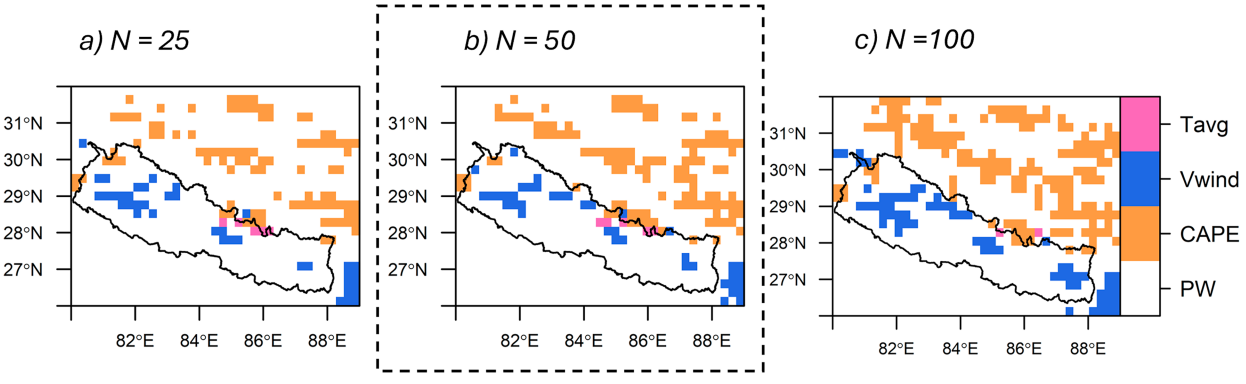

FIG. 6. Sensitivity of the most dominant atmospheric variable driving the 3-day extreme precipitation to the choice of threshold θ. The variables PW, CAPE, V_{wind}, and T_{avg} are represented by the colors white, orange, blue, and pink, respectively.

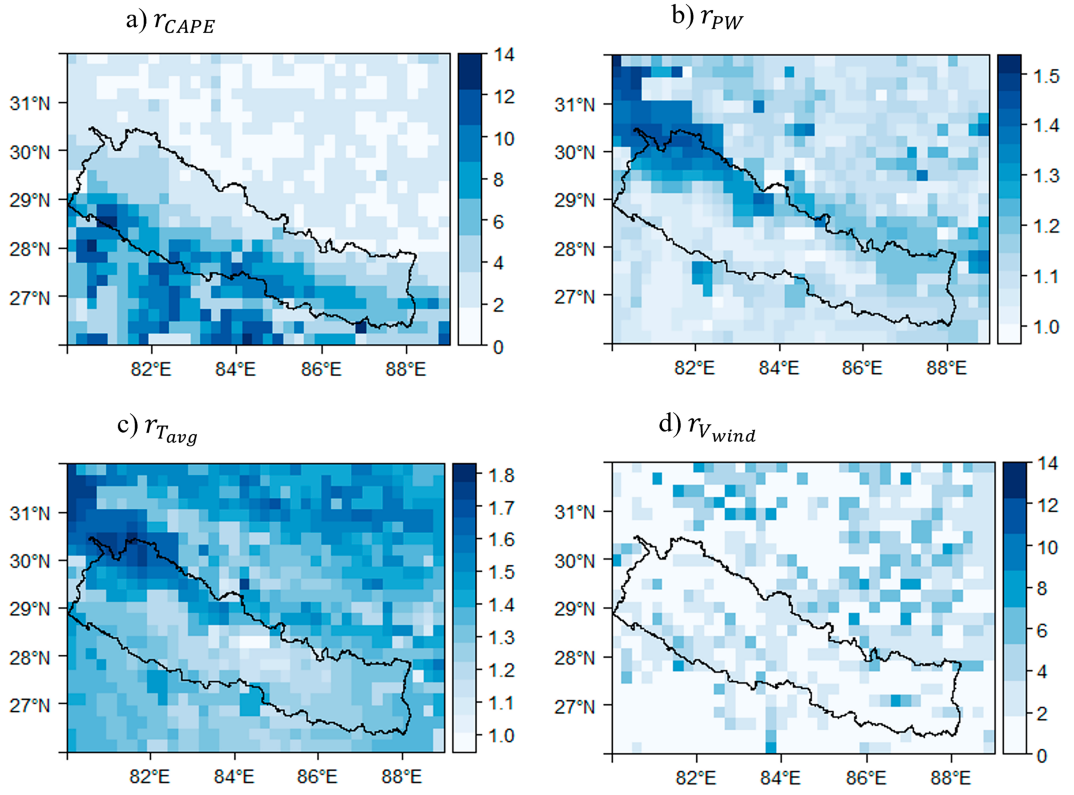

FIG. 7. Spatial distribution of the maximization ratio for (a) CAPE (r_{CAPE}), (b) PW (r_{PW}), (c) T_{avg} ($r_{T_{\mathrm{avg}}}$), and (d) V_{wind}($r_{V_{\mathrm{wind}}}$). Note the different scales.

the maximization ratio for each dominant atmospheric variable is calculated using Eq. (4). In this case study on demonstration of Nepal, the maximization ratios for the four atmospheric variables obtained from the screening process are computed using Eqs. (8)–(11):

$$r_{\mathrm{PW}} = \frac{\mathrm{PW}_{\mathrm{max}}}{\mathrm{PW}_{P\mathrm{max}}}, \tag{8}$$

$$r_{\mathrm{CAPE}} = \frac{\mathrm{CAPE}_{\mathrm{max}}}{\mathrm{CAPE}_{P\mathrm{max}}}, \tag{9}$$

$$r_{v_{\mathrm{wind}}} = \frac{V_{\mathrm{wind}_{\mathrm{max}}}}{V_{\mathrm{wind}_{P\mathrm{max}}}}, \tag{10}$$

$$r_{T_{\mathrm{avg}}} = \frac{T_{\mathrm{avg}_{\mathrm{max}}}}{T_{\mathrm{avg}_{P\mathrm{max}}}}. \tag{11}$$

The spatial distributions of the maximization ratios are presented in Fig. 7. The figure shows that the maximization ratios for PW and T_{avg} are <2, while the ratios for CAPE and V_{wind} are much higher. This is because the variables CAPE and V_{wind} have a broad range of values and a higher upper limit. In this analysis, the negative values of $V_{\mathrm{wind}_{P\mathrm{max}}}$ have been omitted, and the lower limit of the values of $\mathrm{CAPE}_{P\mathrm{max}}$ has been set to 250 J kg^{-1} for better visualization.

Then, the combined maximization ratio (r_{combined}) is calculated as the weighted average of the maximization ratio for each atmospheric variable (weighted by dominance). The combined maximization ratio proposed here is an extension of the moisture maximization approach to include other factors. The simplest form, i.e., a linear expansion of the moisture maximization approach, is proposed here. In this study, r_{combined} is calculated using Eq. (12):

$$r_{\mathrm{combined}} = \frac{(w_{\mathrm{CAPE}} r_{\mathrm{CAPE}} + w_{\mathrm{PW}} r_{\mathrm{PW}} + w_{V_{\mathrm{wind}}} r_{V_{\mathrm{wind}}} + w_{T_{\mathrm{avg}}} r_{T_{\mathrm{avg}}})}{(w_{\mathrm{CAPE}} + w_{\mathrm{PW}} + w_{V_{\mathrm{wind}}} + w_{T_{\mathrm{avg}}})}. \tag{12}$$

1) CORRELATION BETWEEN THE TERMS IN THE COMBINED MAXIMIZATION

The correlation matrix presented in Fig. 8 illustrates the relationships between the weighted terms in the numerator of Eq. (12). The upper triangle of the matrix displays the numeric values of the correlation coefficients between variable pairs, with values indicating the strength and direction of their relationships. The lower triangle of the matrix features scatterplots, which provide insights into the distribution and association between variables. The density plots along the diagonal highlight the probability distribution of each variable, offering a visual representation of how the data are spread. The density

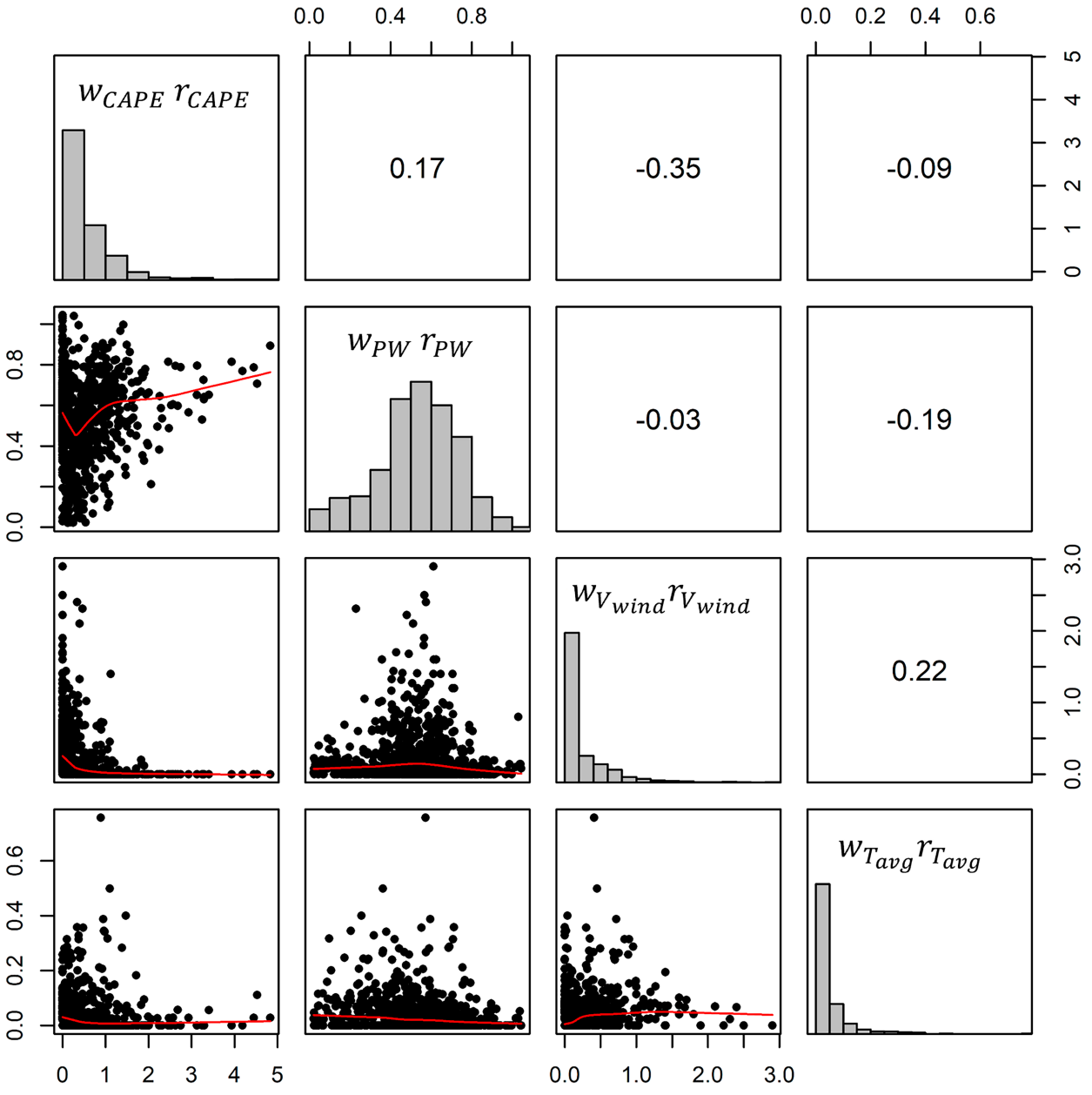

FIG. 8. A correlation plot for the terms included in Eq. (12).

functions suggest that most variables exhibit a right-skewed distribution, meaning that higher values are relatively rare. Overall, most terms show weak correlations, except for a few notable relationships. The $W_{V_{\max}} r_{V_{\max}}$ and $W_{T_{\text{avg}}} r_{T_{\text{avg}}}$ exhibit a weak positive correlation (0.22), suggesting some degree of association between maximum wind speed and average temperature effects. However, the influence of temperature remains relatively independent when compared to other atmospheric factors.

Interestingly, $W_{\text{CAPE}} r_{\text{CAPE}}$ shows a slight negative correlation with $W_{T_{\text{avg}}} r_{T_{\text{avg}}}$ (-0.09) and $W_{\text{PW}} r_{\text{PW}}$ (-0.19), indicating that convective instability and moisture effects may have a distinct role in extreme precipitation events. Additionally, $W_{\text{PW}} r_{\text{PW}}$ and $W_{\text{CAPE}} r_{\text{CAPE}}$ show a positive correlation (0.17), which aligns with previous findings that moisture and convective energy are both key contributors to extreme precipitation.

The comparison reveals that the multifactor maximization approach leads to consistently higher PMP estimates than the moisture maximization approach, highlighting the added value of incorporating a broader set of atmospheric variables in the estimation process. The results emphasize that the multifactor approach accounts for additional factors that contribute to extreme precipitation events, such as convective instability and moisture convergence, leading to more robust and reliable PMP estimates for Nepal.

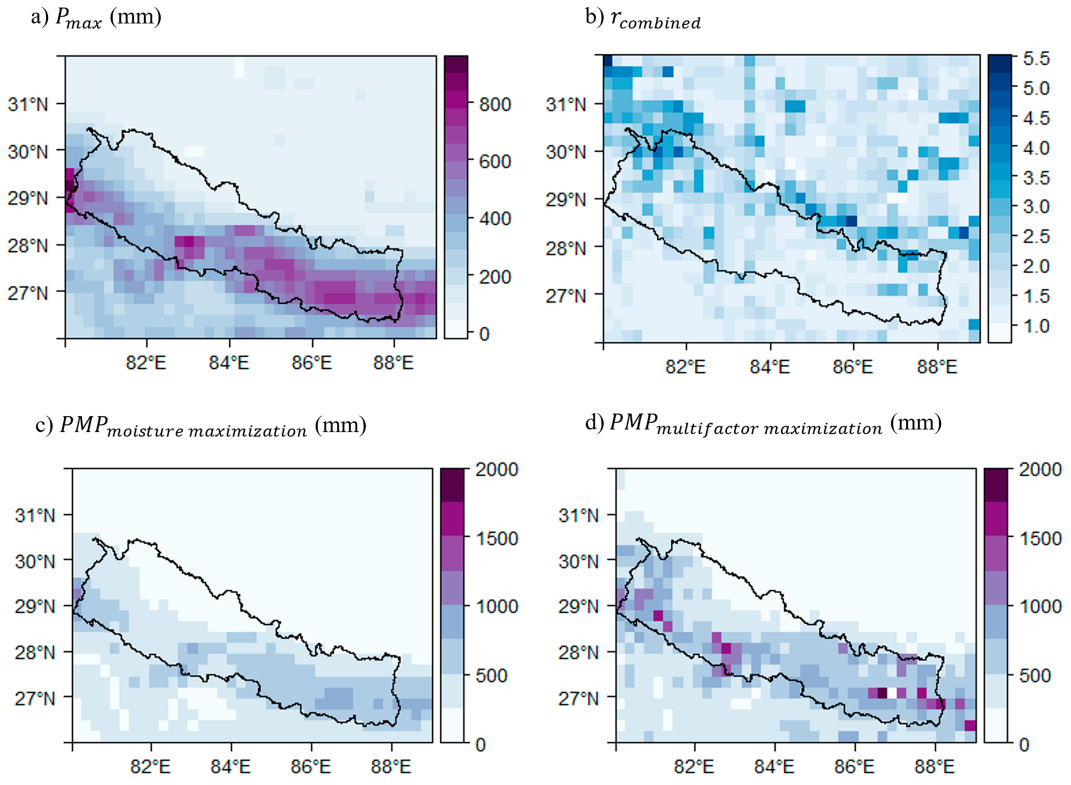

FIG. 9. Illustration of extreme precipitation estimates. (a) The P_{max} is the spatial distribution of the 3-day maximum precipitation observed in the past, (b) r_{combined} is the combined maximization ratio which when multiplied by P_{max} generates the estimate of $\text{PMP}_{\text{multifactor\_maximization}}$, (c) $\text{PMP}_{\text{moisture\_maximization}}$ is the PMP estimate using the moisture maximization approach, and (d) $\text{PMP}_{\text{multifactor\_maximization}}$ is the PMP estimate using the proposed multifactor maximization approach. (c) and (d) are presented on the same scale for easy comparison.

2) PMP ESTIMATION USING THE MULTIFACTOR MAXIMIZATION APPROACH

The PMP estimate is derived by multiplying the combined maximization ratio with the observed maximum precipitation, as shown in Eq. (6). The comparison of the estimates of extreme precipitation in Nepal is presented in Fig. 9, illustrating how different methodologies influence PMP estimation. The maximum 3-day precipitation, P_{max}, observed historically between 1979 and 2019 during the monsoon months is presented in Fig. 9a. The combined maximization ratio, r_{combined}, is presented in Fig. 9b. The estimate of the PMP obtained using the traditional moisture maximization approach estimated with Eq. (1), $\text{PMP}_{\text{moisture\_maximization}}$, is presented in Fig. 9c. The PMP obtained using the proposed multifactor maximization approach with Eq. (6), $\text{PMP}_{\text{multifactor\_maximization}}$, is presented in Fig. 9d. Figures 9c and 9d are presented in the same scale to facilitate direct comparison.

The results indicate that the multifactor maximization approach consistently yields higher PMP estimates than the traditional moisture maximization method across most regions in Nepal. This difference highlights the added value of incorporating multiple atmospheric variables rather than relying solely on moisture availability. The multifactor approach provides a more comprehensive representation of extreme precipitation-generating mechanisms, leading to more robust and potentially more accurate PMP estimates. It is important to note that the high PMP values reflect extreme event scenarios, where all relevant meteorological variables are considered at historically maximum levels, rather than representing typical precipitation events.

Furthermore, the results show spatial variations in PMP estimates, with the multifactor maximization method predicting particularly higher PMP values in regions with strong convective activity and orographic influences. This suggests that extreme precipitation in Nepal may not be solely controlled by moisture availability but is also influenced by dynamic atmospheric conditions that enhance precipitation efficiency.

c. *Comparison of $r_{Combined}$ and r_{PW}*

To assess the influence of incorporating additional atmospheric factors in PMP estimation, we compare the combined maximization ratio (r_{Combined}) with the moisture maximization ratio (r_{PW}), as presented in Fig. 10. This analysis evaluates the extent to which integrating multiple meteorological variables impacts PMP estimates. The ratio of the combined maximization ratio to moisture maximization ratio ($r_{\text{Combined}}/r_{\text{PW}}$) is plotted in Fig. 10. A spatial distribution plotted in Fig. 10a illustrates that it is higher than r_{PW} predominantly in

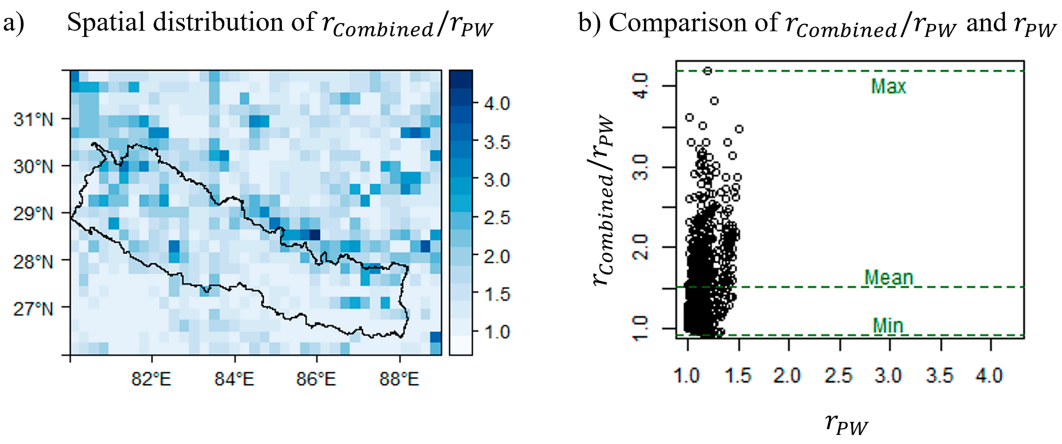

FIG. 10. (a) Spatial distribution of $r_{\text{Combined}}/r_{\text{PW}}$ and (b) comparison of $r_{\text{Combined}}/r_{\text{PW}}$ and r_{PW}.

the region to the north of the Himalayas. This region corresponds to the region where w_{CAPE} is higher. A comparison plot of r_{PW} to $r_{\text{Combined}}/r_{\text{PW}}$ in Fig. 10b illustrates that, on average, the combined maximization ratio is about 1.5 times larger than the moisture maximization ratio, with some values up to 4.2 times larger.

This substantial difference indicates that traditional moisture maximization techniques may underestimate the potential for extreme precipitation, particularly in regions where additional meteorological processes intensify rainfall.

The findings highlight the limitations of solely using moisture maximization for PMP estimation, especially in complex terrain where convective- and synoptic-scale influences are significant. The higher values of r_{Combined} relative to r_{PW} emphasize that moisture availability alone does not fully capture the mechanisms driving extreme precipitation. Instead, the multifactor maximization approach provides a more comprehensive and realistic representation of extreme precipitation potential, offering a refined methodology for PMP estimation in Nepal and other regions with similar meteorological complexities.

d. Limitations

Limitations of the ERA5 dataset used in this study are reflected in the results. ERA5 has been shown to skillfully reproduce PW and precipitation (Tang et al. 2020; Zhang et al. 2019); however, to authors' knowledge, its skill in reproduction of CAPE, V_{wind}, and other variables used in this study has not been studied. ERA5 has been widely used to reproduce the atmospheric processes related to extreme precipitation (Ben Alaya et al. 2019; Bohlinger et al. 2017; Chen and Hossain 2018). We acknowledge that incorporating ground-based observations would strengthen the validation of our findings, and this will be considered in future studies when such data become accessible.

This approach only proposes improvement in 20% of the grid cells. The dominant explanatory variable is presented in Figs. 5 and 6. As seen in the figure, the proposed multifactor maximization method identifies new explanatory variables in 20% of the grid cells; the traditional moisture maximization approach remains unchanged for 80% of the grid cells. In the proposed multifactor maximization method, we individually maximize atmospheric variables and combine them linearly. The possibility of nonlinear covariance, either positive or negative, between atmospheric variables has not been explicitly accounted for. This is because we do not currently have a complete understanding of all the parameters that result in extreme rainfall, and therefore, simplifying assumptions are necessary in the process of PMP estimation and in the process of modeling PMP. As understanding of the driving atmospheric variables and their interrelationships evolves, future research should reevaluate and refine the combination of the variables in this multifactor maximization method.

5. Conclusions

In this study, we explored the states of moisture availability, atmospheric stability, atmospheric humidity, large-scale wind convergence, mean air temperature, temperature gradient, wind direction, and wind magnitude during historical extreme events in Nepal using the ERA5 reanalysis dataset. Building on the work of Chen and Hossain (2018), we identified PW (moisture availability), CAPE (atmospheric stability), and the northward direction of the wind at 850 hPa as the dominant drivers of extreme precipitation in Nepal and calculated the weights of influence of each driver. We then computed the maximization ratio for each atmospheric variable and calculated the combined maximization ratio as the weighted average of the individual maximization ratio.

This study demonstrates that PW is not the only explanatory factor for extreme precipitation. With the screening process presented here, CAPE and northward wind at 850 hPa were identified as important drivers of extreme precipitation in addition to PW. The PMP values estimated using the multifactor approaches were up to 4 times higher than the conventional moisture maximization approach in places where there are multiple drivers of extreme precipitation. The lack of direct influence by T_{avg} is consistent with the observations made by Chen and Hossain (2018) and Kappel et al. (2020) in the United States and Lang et al. (2022) in central China.

However, an increase (or decrease) in temperature has the potential to affect other atmospheric variables, which in turn may influence extreme precipitation.

Although zonal wind is a commonly considered driver in other regions, its influence in Nepal is minimal due to the region's complex topography. Particularly, in the Himalayas, the orographic effects of the mountains dominate atmospheric circulation, leading to more localized wind patterns that are less influenced by zonal wind. As a result, moisture availability, atmospheric stability (CAPE), and wind direction at 850 hPa play more prominent roles in driving extreme precipitation in Nepal.

The strength of this approach is its ability to capture underlying atmospheric variables driving extreme precipitation at a seasonal and local scale, while retaining the essential form and interpretability of the conventional moisture maximization approach to PMP estimation. This makes the multifactor maximization approach widely applicable for PMP estimation. We expect that the identity and spatial distribution of the dominant atmospheric variable would need to be reassessed in application of this procedure to a different location. Beyond the implications for protection of life and property, a spatially generalizable improvement in PMP estimation would benefit water resources project planning (e.g., Rodríguez et al. 2021), operational hydrology (e.g., Zhu et al. 2021; Atreya et al. 2024), and utilities engaged in source water protection from water contamination events (e.g., Behzadi et al. 2022; Rahat et al. 2023). The institutions responsible for water systems planning, operation, and emergency response nearly all adopt the conventional moisture maximization approach described in this paper.

Numerical-model-based PMP methodologies represent a pathway for improvement of conventional moisture maximization methodologies, and recent studies have compared the performance of numerical-model-based methods to the conventional approach (e.g., Ohara et al. 2011; Hiraga and Meza 2025). Findings from Hiraga and Meza (2025) suggest that the conventional method overestimates the 72-h PMP. Our study suggests that the conventional moisture maximization approach underestimates PMP. Further studies comparing numerical-model-based PMP estimation methodologies to conventional methodologies are needed to encourage a shift in standard practice, if such a shift is warranted by the accuracy–effort trade-off (i.e., if the additional effort required by the numerical model approach is justified by the improved accuracy in PMP estimation).

Studies of PMP under climate change have evaluated the effect of increasing temperature on moisture availability (Ishida et al. 2018; Beauchamp et al. 2013; Rouhani and Leconte 2018). However, these only capture the thermodynamic effect of climate change and underrepresent the uncertainty that arises from the effect of temperature increase on other atmospheric processes. Hiraga et al. (2025) developed a novel dynamic-model-based method to estimate PMP, showing that nonlinear precipitation responses to warming are well explained by changes to integrated water vapor transport (IVT) and vertically integrated moisture flux convergence (VIMFC). With the advancement in the understanding of the effect of temperature on other drivers of extreme precipitation (e.g., inclusion of IVT and VIMFC), the multifactor maximization method presented here can be used to approximate PMP under climate change.

In this work, we have evaluated hydrometeorological variables on a gridcell (localized) basis. We have not accounted for synoptic-scale precipitation drivers (e.g., low pressure systems) and teleconnections to locations of precipitation (e.g., Rahat et al. 2022; Steinschneider et al. 2019). An exploration of these systems would help to identify moisture sources and show which synoptic-scale systems are responsible for PMP. The insights provided by an exploration of this type would be relevant to climate change analyses. General circulation models (GCMs) could be applied to inform the likelihoods of synoptic-level pressure changes on potential future PMP.

Acknowledgments. This research was supported by a grant from the World Bank Group (Contract 7202026), for a project entitled, "Support to World Banks Risk Assessment of Hydrologic Variability in Upper Arun Basin." The authors gratefully acknowledge the support of Pravin Karki, Nick Mandeville, and others who influenced our strategy for the evaluation of precipitation extremes in the region. We also benefited from the generous support of the Ohio Supercomputer Center (OSC).

Data availability statement. All the meteorological data used in this study (ERA5) are openly available from the Climate Data Store at https://cds.climate.copernicus.eu/#!/home, and the database of hydropower plants in Nepal is openly available at https://www.doed.gov.np/license/54.

REFERENCES

ADB, 2019: Nepal: Flood Risk Sector Assessment: TA9634-REG: Strengthening Integrated Flood Risk Management. Asian Development Bank, Consultant Rep., 89 pp.

Agrawala, S., V. Raksakulthai, M. van Aalst, P. Larsen, J. Smith, and J. Reynolds, 2003: *Development and Climate Change in Nepal: Focus on Water Resources and Hydropower.* OCED, 64 pp.

Atreya, G., E. Emery, N. Rogacki, M. Buck, R. Soltanian, D. McAvoy, and P. Ray, 2024: Estimating the influence of water control infrastructure on natural low flow in complex reservoir systems: A case study of the Ohio River. *J. Hydrol.*, **54**, 101897, https://doi.org/10.1016/j.ejrh.2024.101897.

Beard, L. R., 1962: *Statistical Methods* in *Hydrology.* Army Engineer District, 118 pp.

Beauchamp, J., R. Leconte, M. Trudel, and F. Brissette, 2013: Estimation of the summer-fall PMP and PMF of a northern watershed under a changed climate. *Water Resour. Res.*, **49**, 3852–3862, https://doi.org/10.1002/wrcr.20336.

Behzadi, F., A. Wasti, T. E. Steissberg, and P. A. Ray, 2022: Vulnerability assessment of drinking water supply under climate uncertainty using a river contamination risk (RANK) model. *Environ. Modell. Software*, **150**, 105294, https://doi.org/10.1016/j.envsoft.2021.105294.

Ben Alaya, M. A., F. Zwiers, and X. Zhang, 2018: Probable maximum precipitation: Its estimation and uncertainty

quantification using bivariate extreme value analysis. *J. Hydrometeor.*, **19**, 679–694, https://doi.org/10.1175/JHM-D-17-0110.1.

——, ——, and ——, 2019: Evaluation and comparison of CanRCM4 and CRCM5 to estimate probable maximum precipitation over North America. *J. Hydrometeor.*, **20**, 2069–2089, https://doi.org/10.1175/JHM-D-18-0233.1.

Bohlinger, P., and A. Sorteberg, 2018: A comprehensive view on trends in extreme precipitation in Nepal and their spatial distribution. *Int. J. Climatol.*, **38**, 1833–1845, https://doi.org/10.1002/joc.5299.

——, ——, and H. Sodemann, 2017: Synoptic conditions and moisture sources actuating extreme precipitation in Nepal. *J. Geophys. Res. Atmos.*, **122**, 12 653–12 671, https://doi.org/10.1002/2017JD027543.

Boota, M. W., G. Nabi, T. Abbas, H. Jin, A. Yousaf, and M. A. Boota, 2018: Comparative study of probable maximum precipitation and isohyetal maps for mountainous regions, Pakistan. *Sci. Cold Arid Reg.*, **10**, 55–68.

Chen, X., and F. Hossain, 2018: Understanding model-based probable maximum precipitation estimation as a function of location and season from atmospheric reanalysis. *J. Hydrometeor.*, **19**, 459–475, https://doi.org/10.1175/JHM-D-17-0170.1.

——, ——, and L. R. Leung, 2017: Probable maximum precipitation in the U.S. Pacific Northwest in a changing climate. *Water Resour. Res.*, **53**, 9600–9622, https://doi.org/10.1002/2017WR021094.

Coelho, G. D. A., C. M. Ferreira, J. Johnston, J. L. Kinter III, I. J. Dollan, and V. Maggioni, 2022: Potential impacts of future extreme precipitation changes on flood engineering design across the contiguous United States. *Water Resour. Res.*, **58**, e2021WR031432, https://doi.org/10.1029/2021WR031432.

Corte-Real, J., B. Qian, and H. Xu, 1998: Regional climate change in Portugal: Precipitation variability associated with large-scale atmospheric circulation. *Int. J. Climatol.*, **18**, 619–635, https://doi.org/10.1002/(SICI)1097-0088(199805)18:6<619::AID-JOC271>3.0.CO;2-T.

Dawdy, D. R., V. W. Griffis, and V. K. Gupta, 2012: Regional flood-frequency analysis: How we got here and where we are going. *J. Hydrol. Eng.*, **17**, 953–959, https://doi.org/10.1061/(ASCE)HE.1943-5584.0000584.

Dee, D. P., and Coauthors, 2011: The ERA-Interim reanalysis: Configuration and performance of the data assimilation system. *Quart. J. Roy. Meteor. Soc.*, **137**, 553–597, https://doi.org/10.1002/qj.828.

Department of Electricity Development, 2022: License of hydropower plants in Nepal. https://www.doed.gov.np/license/54.

Ding, G., and Coauthors, 2019: A time-trend ecological study for identifying flood-sensitive infectious diseases in Guangxi, China from 2005 to 2012. *Environ. Res.*, **176**, 108577, https://doi.org/10.1016/j.envres.2019.108577.

Dupont, J.-C., M. Haeffelin, P. Drobinski, and T. Besnard, 2008: Parametric model to estimate clear-sky longwave irradiance at the surface on the basis of vertical distribution of humidity and temperature. *J. Geophys. Res.*, **113**, D07203, https://doi.org/10.1029/2007JD009046.

England, J. F. Jr., T. A. Cohn, B. A. Faber, J. R. Stedinger, W. O. Thomas, Jr., A. G. Veilleux, J. E. Kiang, and R. R. Mason Jr., 2019: Guidelines for determining flood flow frequency—Bulletin 17C. U.S. Geological Survey Techniques and Methods 4–B5, 148 pp.

FEMA, 2013: Selecting and Accommodating Inflow Design Floods for Dams (FEMA P-94). FEMA, 47 pp., https://www.fema.gov/emergency-managers/risk-management/dam-safety/federal-guidelines.

Fischer, E. M., and R. Knutti, 2016: Observed heavy precipitation increase confirms theory and early models. *Nat. Climate Change*, **6**, 986–991, https://doi.org/10.1038/nclimate3110.

Fluixa-Sanmartin, J., L. Altarejos-Garcia, A. Morales-Torres, and I. Escuder-Bueno, 2018: Review article: Climate change impacts on dam safety. *Nat. Hazards Earth Syst. Sci.*, **18**, 2471–2488, https://doi.org/10.5194/nhess-18-2471-2018.

Foster, H. A., 1924: Theoretical frequency curves and their application to engineering problem. *Trans. Amer. Soc. Civ. Eng.*, **87**, 142–173, https://doi.org/10.1061/TACEAT.0003398.

Fuller, W. E., 1914: Flood flows. *Trans. Amer. Soc. Civ. Eng.*, **77**, 564–617, https://doi.org/10.1061/taceat.0002552.

Gumbel, E. J., and V. T. Chow, 1952: Discussion of "a general formula for hydrologic frequency analysis". *Eos, Trans. Amer. Geophys. Union*, **33**, 277–282, https://doi.org/10.1029/TR033i002p00277.

Hansen, E. M., L. C. Schreiner, and J. F. Miller, 1982: Application of probable maximum precipitation estimates: United States east of the 105th meridian. Hydrometeorol. Rep. 52, 182 pp., https://repository.library.noaa.gov/view/noaa/7046.

Hersbach, H., and Coauthors, 2020: The ERA5 global reanalysis. *Quart. J. Roy. Meteor. Soc.*, **146**, 1999–2049, https://doi.org/10.1002/qj.3803.

Hershfield, D. M., 1961: Estimating the probable maximum precipitation. *J. Hydraul. Div., Amer. Soc. Civ. Eng.*, **87**, 99–116.

——, 1965: Method for estimating probable maximum rainfall. *J. Amer. Water Works Assoc.*, **57**, 965–972, https://doi.org/10.1002/j.1551-8833.1965.tb01486.x.

Hiraga, Y., and J. Meza, 2025: Extreme precipitation modeling and probable maximum precipitation (PMP) estimation in Chile. *J. Hydrol.*, **58**, 102274, https://doi.org/10.1016/j.ejrh.2025.102274.

——, Y. Iseri, M. D. Warner, C. D. Frans, A. M. Duren, J. F. England, and M. L. Kavvas, 2021: Estimation of long-duration maximum precipitation during a winter season for large basins dominated by atmospheric Rivers using a numerical weather model. *J. Hydrol.*, **598**, 126224, https://doi.org/10.1016/j.jhydrol.2021.126224.

——, ——, ——, A. M. Duren, J. F. England, C. D. Frans, and M. L. Kavvas, 2024a: Model-based estimation of long-duration design precipitation for basins with large storage volumes of reservoirs and snowpacks. *J. Flood Risk Manage.*, **17**, e12992, https://doi.org/10.1111/jfr3.12992.

——, ——, ——, ——, ——, and M. Levent Kavvas, 2024b: Response of precipitation increases to changes in atmospheric moisture and its flux in the Columbia River Basin: WRF model–based precipitation maximization for PMP studies. *J. Hydrol. Eng.*, **29**, 04024014, https://doi.org/10.1061/JHYEFF.HEENG-6169.

——, R. Tahara, and J. Meza, 2025: A methodology to estimate probable maximum precipitation (PMP) under climate change using a numerical weather model. *J. Hydrol.*, **652**, 132659, https://doi.org/10.1016/j.jhydrol.2024.132659.

Hurford, A. P., J. J. Harou, L. Bonzanigo, P. A. Ray, P. Karki, L. Bharati, and P. Chinnasamy, 2020: Efficient and robust hydropower system design under uncertainty—A demonstration in Nepal. *Renew. Sustain. Energy Rev.*, **132**, 109910, https://doi.org/10.1016/j.rser.2020.109910.

ICOLD, 2018: *Flood Evaluation and Dam Safety*. CRC Press, 306 pp., https://doi.org/10.1201/9781351031103.

ICWR, 1966: *Methods of Flow Frequency Analysis.* U.S. Government Printing Office, 42 pp.

IFRC, 2015: World disaster report 2015: Focus on local actors, the key to humanitarian effectiveness. International Federation of Red Cross and Red Crescent Societies, 270 pp.

Ishida, K., N. Ohara, M. L. Kavvas, Z. Q. Chen, and M. L. Anderson, 2018: Impact of air temperature on physically-based maximum precipitation estimation through change in moisture holding capacity of air. *J. Hydrol.*, **556**, 1050–1063, https://doi.org/10.1016/j.jhydrol.2016.10.008.

Jeuken, A., and Coauthors, 2023: Challenges for upscaling hydrological effectiveness of nature-based solution for adaptation to climate change in watersheds. *Aquat. Ecosyst. Health Manage.*, **26**, 19–32, https://doi.org/10.14321/aehm.026.02.019.

Kappel, W. D., D. M. Hultstrand, K. Steinhilber, and J. T. Rodel, 2020: Climate change and PMP: Are these storms changing? *J. Dam Safety*, **17**, 6–20.

——, ——, J. T. Rodel, G. A. Muhlestein, and K. Steinhilber, 2022: North Dakota interim guidance: Using the probable maximum precipitation study. North Dakota Dept. of Water Resources Rep., Bismark, ND, 10 pp., https://www.dwr.nd.gov/pdfs/pmp_interim_guidance.pdf.

——, ——, ——, ——, M. Venticinque, and K. Steinhilber, June 2023: Statewide Probable Maximum Precipitation for New Jersey. New Jersey Department of Environmental Protection Dam Safety Final Rep., 144 pp., https://dep.nj.gov/wp-content/uploads/wlm/downloads/damsafety/probable-maximum-precipitation-study-for-new-jersey-final_2025.pdf.

Khadka, A., P. Wagnon, F. Brun, D. Shrestha, Y. Lejeune, and Y. Arnaud, 2022: Evaluation of ERA5-Land and HARv2 reanalysis data at high elevation in the upper Dudh Koshi basin (Everest region, Nepal). *J. Appl. Meteor. Climatol.*, **61**, 931–954, https://doi.org/10.1175/JAMC-D-21-0091.1.

Kucharski, J., S. Steinschneider, J. Herman, J. Olszewski, W. Arnold, S. Rahat, R. Maendley, and P. Ray, 2024: Bridging the gap between top-down and bottom-up climate vulnerability assessments: Process informed exploratory scenarios identify system-based water resource vulnerabilities. *Water Resour. Res.*, **60**, e2023WR036649, https://doi.org/10.1029/2023WR036649.

Kumar, K. K., B. Rajagopalan, and M. A. Cane, 1999: On the weakening relationship between the Indian monsoon and ENSO. *Science*, **284**, 2156–2159, https://doi.org/10.1126/science.284.5423.2156.

Kunkel, K. E., T. R. Karl, D. R. Easterling, K. Redmond, J. Young, X. Yin, and P. Hennon, 2013: Probable maximum precipitation and climate change. *Geophys. Res. Lett.*, **40**, 1402–1408, https://doi.org/10.1002/grl.50334.

Lang, Y., Z. Jiang, and X. Wu, 2022: Investigating the linkage between extreme rainstorms and concurrent synoptic features: A case study in Henan, Central China. *Water*, **14**, 1065, https://doi.org/10.3390/w14071065.

Lavers, D. A., A. Simmons, F. Vamborg, and M. J. Rodwell, 2022: An evaluation of ERA5 precipitation for climate monitoring. *Quart. J. Roy. Meteor. Soc.*, **148**, 3152–3165, https://doi.org/10.1002/qj.4351.

Lee, O., and S. Kim, 2018: Estimation of future probable maximum precipitation in Korea using multiple regional climate models. *Water*, **10**, 637, https://doi.org/10.3390/w10050637.

——, Y. Park, E. S. Kim, and S. Kim, 2016: Projection of Korean probable maximum precipitation under future climate change scenarios. *Adv. Meteor.*, **2016**, 3818236, https://doi.org/10.1155/2016/3818236.

Lepore, C., D. Veneziano, and A. Molini, 2015: Temperature and CAPE dependence of rainfall extremes in the eastern United States. *Geophys. Res. Lett.*, **42**, 74–83, https://doi.org/10.1002/2014GL062247.

Li, C., J. Liu, F. Du, F. W. Zwiers, and G. Feng, 2025: Increasing certainty in projected local extreme precipitation change. *Nat. Commun.*, **16**, 850, https://doi.org/10.1038/s41467-025-56235-9.

Liang, S. Y, and N. Messenger, 2018: Infectious diseases after hydrologic disasters. *Emerg. Med. Clin. North Amer.*, **36**, 835–851, https://doi.org/10.1016/j.emc.2018.07.002.

Liu, R., X. Zhang, W. Wang, Y. Wang, H. Liu, M. Ma, and G. Tang, 2024: Global-scale ERA5 product precipitation and temperature evaluation. *Ecol. Indic.*, **166**, 112481, https://doi.org/10.1016/j.ecolind.2024.112481.

Loriaux, J. M., G. Lenderink, and A. P. Siebesma, 2016: Peak precipitation intensity in relation to atmospheric conditions and large-scale forcing at midlatitudes. *J. Geophys. Res. Atmos.*, **121**, 5471–5487, https://doi.org/10.1002/2015JD024274.

Loucks, D. P., and E. van Beek, 2017: *Water Resource Systems Planning and Management: An Introduction to Methods, Models, and Applications.* Springer International Publishing, 624 pp., https://doi.org/10.1007/978-3-319-44234-1.

——, J. R. Stedinger, and D. A. Haith, 1981: *Water Resource Systems Planning and Analysis.* Prentice Hall, 559 pp.

Luo, Y., L. Wang, C. Hu, L. Hao, and G. Sun, 2024: Changing extreme precipitation patterns in Nepal over 1971–2015. *Earth Space Sci.*, **11**, e2024EA003563, https://doi.org/10.1029/2024EA003563.

Maidment, D. R., 1993: *Handbook of Hydrology.* McGraw-Hill, 1424 pp.

Marchau, V. A., W. E. Walker, P. J. Bloemen, and S. W. Popper, 2019: *Decision Making Under Deep Uncertainty: From Theory to Practice*. Springer, 405 pp.

Mays, L. W., 2010: *Water Resources Engineering.* 2nd ed. John Wiley and Sons, 928 pp.

Michalak, A. M., 2016: Study role of climate change in extreme threats to water quality. *Nature*, **535**, 349–350, https://doi.org/10.1038/535349a.

Micovic, Z., M. G. Schaefer, and G. H. Taylor, 2015: Uncertainty analysis for probable maximum precipitation estimates. *J. Hydrol.*, **521**, 360–373, https://doi.org/10.1016/j.jhydrol.2014.12.033.

Mukhopadhyay, B., and W. D. Kappel, 2016: Probable maximum precipitation. *Handbook of Applied Hydrology*, 2nd ed. V. P. Singh, Ed., McGraw-Hill Education, 126-1–126-18.

Najibi, N., S. Mukhopadhyay, and S. Steinschneider, 2021: Identifying weather regimes for regional-scale stochastic weather generators. *Int. J. Climatol.*, **41**, 2456–2479, https://doi.org/10.1002/joc.6969.

NASEM, 2024: *Modernizing Probable Maximum Precipitation Estimation*. The National Academies Press, 212 pp., https://doi.org/10.17226/27460.

Nazarian, R. H., J. V. Vizzard, C. P. Agostino, and N. J. Lutsko, 2022: Projected changes in future extreme precipitation over the northeast United States in the NA-CORDEX ensemble. *J. Appl. Meteor. Climatol.*, **61**, 1649–1668, https://doi.org/10.1175/JAMC-D-22-0008.1.

NWS, 2015: Regions covered by different NWS PMP documents (as of 2015). Accessed 1 May 2022, https://www.nws.noaa.gov/oh/hdsc/studies/pmp.html.

Ohara, N., M. L. Kavvas, S. Kure, Z. Q. Chen, S. Jang, and E. Tan, 2011: Physically based estimation of maximum precipitation over American River watershed, California.

J. Hydrol. Eng., **16**, 351–361, https://doi.org/10.1061/(ASCE)HE.1943-5584.0000324.

Papalexiou, S. M., 2018: Unified theory for stochastic modelling of hydroclimatic processes: Preserving marginal distributions, correlation structures, and intermittency. *Adv. Water Resour.*, **115**, 234–252, https://doi.org/10.1016/j.advwatres.2018.02.013.

Rahat, S. H., and Coauthors, 2022: Characterizing hydrologic vulnerability under nonstationary climate and antecedent conditions using a process-informed stochastic weather generator. *J. Water Resour. Plann. Manage.*, **148**, 04022028, https://doi.org/10.1061/(ASCE)WR.1943-5452.0001557.

——, and Coauthors, 2023: Remote sensing-enabled machine learning for river water quality modeling under multidimensional uncertainty. *Sci. Total Environ.*, **898**, 165504, https://doi.org/10.1016/j.scitotenv.2023.165504.

——, and Coauthors, 2024: Bracing for impact: How shifting precipitation extremes may influence physical climate risks in an uncertain future. *Sci. Rep.*, **14**, 17398, https://doi.org/10.1038/s41598-024-65618-9.

Rastogi, D., and Coauthors, 2017: Effects of climate change on probable maximum precipitation: A sensitivity study over the Alabama-Coosa-Tallapoosa River Basin. *J. Geophys. Res. Atmos.*, **122**, 4808–4828, https://doi.org/10.1002/2016JD026001.

Ray, P. A., L. Bonzanigo, S. Wi, E. Yang, P. Karki, L. E. García, D. J. Rodriguez, and C. M. Brown, 2018: Multidimensional stress test for hydropower investments facing climate, geophysical and financial uncertainty. *Global Environ. Change*, **48**, 168–181, https://doi.org/10.1016/j.gloenvcha.2017.11.013.

——, M. Ü. Taner, K. E. Schlef, S. Wi, H. F. Khan, S. S. G. Freeman, and C. M. Brown, 2019: Growth of the decision tree: Advances in bottom-up climate change risk management. *J. Amer. Water Resour. Assoc.*, **55**, 920–937, https://doi.org/10.1111/1752-1688.12701.

Robertson, A. W., and M. Ghil, 1999: Large-scale weather regimes and local climate over the western United States. *J. Climate*, **12**, 1796–1813, https://doi.org/10.1175/1520-0442(1999)012<1796:LSWRAL>2.0.CO;2.

Rodríguez, D. J., H. A. Paltán, L. E. García, P. A. Ray, and S. S. G. Freeman, 2021: Water-related infrastructure investments in a changing environment: A perspective from the world bank. *Water Policy*, **23**, 31–53, https://doi.org/10.2166/wp.2021.265.

Rouhani, H., and R. Leconte, 2018: A methodological framework to assess PMP and PMF in snow-dominated watersheds under changing climate conditions—A case study of three watersheds in Québec (Canada). *J. Hydrol.*, **561**, 796–809, https://doi.org/10.1016/j.jhydrol.2018.04.047.

Rousseau, A. N., I. M. Klein, D. Freudiger, P. Gagnon, A. Frigon, and C. Ratte-Fortin, 2014: Development of a methodology to evaluate probable maximum precipitation (PMP) under changing climate conditions: Application to southern Quebec, Canada. *J. Hydrol.*, **519**, 3094–3109, https://doi.org/10.1016/j.jhydrol.2014.10.053.

Salas, J. D., M. L. Anderson, S. M. Papalexiou, and F. Frances, 2020: PMP and climate variability and change: A review. *J. Hydrol. Eng.*, **25**, 03120002, https://doi.org/10.1061/(ASCE)HE.1943-5584.0002003.

Shrestha, A. B., C. P. Wake, J. E. Dibb, and P. A. Mayewski, 2000: Precipitation fluctuations in the Nepal Himalaya and its vicinity and relationship with some large scale climatological parameters. *Int. J. Climatol.*, **20**, 317–327, https://doi.org/10.1002/(SICI)1097-0088(20000315)20:3<317::AID-JOC476>3.0.CO;2-G.

Sigdel, M., and M. Ikeda, 2012: Summer monsoon rainfall over Nepal related with large scale atmospheric circulations. *J. Earth Sci. Climate Change*, **3**, 112, https://doi.org/10.4172/2157-7617.1000112.

Steinschneider, S., P. Ray, S. H. Rahat, and J. Kucharski, 2019: A weather-regime-based stochastic weather generator for climate vulnerability assessments of water systems in the western United States. *Water Resour. Res.*, **55**, 6923–6945, https://doi.org/10.1029/2018WR024446.

Stoffel, M., and C. Huggel, 2012: Effects of climate change on mass movements in mountain environments. *Prog. Phys. Geogr. Earth Environ.*, **6**, 421–439, https://doi.org/10.1177/0309133312441010.

Stratz, S. A., and F. Hossain, 2014: Probable maximum precipitation in a changing climate: Implications for dam design. *J. Hydrol. Eng.*, **19**, 06014006, https://doi.org/10.1061/(ASCE)HE.1943-5584.0001021.

Suman, M., and R. Maity, 2020: Southward shift of precipitation extremes over South Asia: Evidences from CORDEX data. *Sci. Rep.*, **10**, 6452, https://doi.org/10.1038/s41598-020-63571-x.

Tang, G., M. P. Clark, S. M. Papalexiou, Z. Ma, and Y. Hong, 2020: Have satellite precipitation products improved over last two decades? A comprehensive comparison of GPM IMERG with nine satellite and reanalysis datasets. *Remote Sens. Environ.*, **240**, 111697, https://doi.org/10.1016/j.rse.2020.111697.

Tarouilly, E. G., K. D. Holman, and D. P. Lettenmaier, 2024: A physically constrained model-based moisture amplification approach for probable maximum precipitation (PMP) estimation. *J. Hydrometeor.*, **25**, 1407–1420, https://doi.org/10.1175/JHM-D-23-0204.1.

Thomas, W. O., Jr., 1985: A uniform technique for flood frequency analysis. *J. Water Resour. Plann. Manage.*, **111**, 321–337, https://doi.org/10.1061/(ASCE)0733-9496(1985)111:3(321).

Trenberth, K. E. 2011: Changes in precipitation with climate change. *Climate Res.*, **47**, 123–138, https://doi.org/10.3354/cr00953.

UNDRR, 2025: Resilience pays: Financing and investing for our future. Global Assessment Report on Disaster Risk Reduction, United Nations Office for Disaster Risk Reduction, 283 pp.

US Weather Bureau, 1960: Generalized estimates of probable maximum precipitation for the United States west of the 105th meridian for areas to 400 square miles and durations to 24 hours. US Department of Commerce Tech. Paper 38, 82 pp., https://www.weather.gov/media/owp/oh/hdsc/docs/TP38.pdf.

Wang, S.-Y., and R. R. Gillies, 2013: Influence of the Pacific quasi-decadal oscillation on the monsoon precipitation in Nepal. *Climate Dyn.*, **40**, 95–107, https://doi.org/10.1007/s00382-012-1376-2.

Wasti, A., P. Ray, S. Wi, C. Folch, M. Ubierna, and P. Karki, 2022: Climate change and the hydropower sector: A global review. *Wiley Interdiscip. Rev.: Climate Change*, **13**, e757, https://doi.org/10.1002/wcc.757.

WMO, 2009: Manual on estimation of Probable Maximum Precipitation (PMP). Tech. Rep. WMO-1045, 257 pp., https://library.wmo.int/viewer/35708/#page=1&viewer=picture&o=bookmarks&n=0&q=.

WRI, 2015: World's 15 countries with the most people exposed to river floods. World Resources Institute, https://www.wri.org/insights/worlds-15-countries-most-people-exposed-river-floods.

Yang, L., and J. Smith, 2018: Sensitivity of extreme rainfall to atmospheric moisture content in the arid/semiarid southwestern United States: Implications for probable maximum precipitation estimates. *J. Geophys. Res. Atmos.*, **123**, 1638–1656, https://doi.org/10.1002/2017JD027850.

Zhang, Y., C. Cai, B. Chen, and W. Dai, 2019: Consistency evaluation of precipitable water vapor derived from ERA5, ERA-interim, GNSS, and radiosondes over China. *Radio Sci.*, **54**, 561–571, https://doi.org/10.1029/2018RS006789.

Zhou, Y., Z. Liang, Y. Hu, D. Li, T. Liu, and X. Lei, 2020: An improved moisture and wind maximization method for probable maximum precipitation estimation and its application to a small catchment in China. *Int. J. Climatol.*, **40**, 2624–2638, https://doi.org/10.1002/joc.6355.

Zhu, Z., A. Wasti, T. Schade, and P. A. Ray, 2021: Techniques to evaluate the modifier process of National Weather Service flood forecasts. *J. Hydrol. X*, **11**, 100073, https://doi.org/10.1016/j.hydroa.2020.100073.

Zielinski, P. A., 2009: Safety of dams, probable maximum flood, and the selection of inflow design floods. *Paper Presented at the CDA 2009 Annual Conf.*, Edmonton, Alberta, Canada, Canadian Dam Association, 1–13, https://www.osti.gov/etdeweb/biblio/21245444.